CHALMERS

Mutually commutated converter equipped with thyristor-based cycloconverter

Master of Science Thesis

Zhao Shuang

MSc in Electric Power Engineering 60p (Degree of Civilingenjörsexamen, eq. 180p)
Department of Electric Power Engineering
Division of Energy and Environment
CHALMERS UNIVERSITY OF TECHNOLOGY
Göteborg, Sweden, 2008

Mutually commutated converter equipped with thyristor-based cycloconverter

Zhao Shuang

Master of Science Thesis

Supervisor:
Dr. Staffan Norrga

Examiner:
Prof. Torbjörn Thiringer

XR-EE-EME 2008:???

Department of Energy and Environment
Division of Electric Power Engineering
CHALMERS UNIVERSITY OF TECHNOLOGY
Göteborg, Sweden, 2008

Abstract

The switching losses of power conversion systems can be significantly reduced by use of the proposed mutually commutated converter topologies which equipped with IGBT-based cycloconverters and permit soft switching of all semiconductor valves in all operating points without any auxiliary valves. However, due to the inherent properties, thyristors are more suitable and attractive for such naturally commutated converters.

A simplified three phase power conversion system is studied in this thesis where the load side is represented by counter-emf. The aim of the thesis is to find a feasible way which allows the thyristor-based cycloconverter to be commutated at any instant of each modulation interval. With this purpose, the method should be able to overcome the inherit limitation of the thyristor, which is the lack of turn-off capability.

A proposed modulation method named “current clamping control strategy” for wind farms is studied and analyzed using in different operating points in this thesis. Furthermore, the cascaded topology is discussed to show the superiority with respect to the total harmonic distortion.

Key words: mutually commutated converter, cycloconverter, current clamping

Acknowledgement

This work was carried out under supervision of Dr. Staffan Norrga at the Division of Power Technologies at ABB Corporate Research in Västerås. His valuable guidance in performing this work is gratefully appreciated. Without his help, this work would not be possible. And I would also like to express my highest gratitude to him for the great opportunity he offered me to continues working in ABB.

I also want to thank Mr. Stephan Meier, who did a great job in his research and generously shared his productions with me. My thesis would not move on without his previous work.

A special thank also goes to Prof. Torbjörn Thiringer who carefully checked and corrected my report during his busy and precious time.

And my dear friend, Mr. Liu Zongyu, please accept my honest appreciation. Thank you for being with me throughout my darkest time and never abandon me when I was endlessly complaining.

Last but certainly not least, I would like to give my greatest indebted to my dearest fiancée Liu Jingjing. Thank you for your support and keeping up my spirit, the life with you is full of light.

I dedicate this thesis to my mother and father.

Västerås, March 2008

Zhao Shuang

List of Symbols

Symbol	*Quality*	*Unit*
e	Natural base (≈2.7182818…)	-
π	Constant (≈3.14159265...)	-
j	Imaginary unit (j^2=-1)	-
t	Time	s
$\overline{u}$	Voltage space vector, instantaneous value	-
$\overline{i}$	Current Voltage space vector, instantaneous value	-
$\overline{e}$	Counter-emf space vector, instantaneous value	-
$\hat{U}$	Peak AC value	V
i_i	Phase currents (i=1,2,3)	A
i_{tr}	Transformer current (VSC winding)	A
I	Current value in steady-state	A
u	Voltage	V
u_i	Phase voltages (i=1,2,3)	V
u_{tr}	Transformer voltage (VSC winding)	V
U_d, V_{dc}	Converter DC link voltage	V
U_q	Magnitude of phase voltage pulses	V
e_i	Counter-emfs, instantaneous values (i=1,2,3)	V
E	Magnitude of counter-emf in steady-state	V
v_M	Potential of the neutral point	V
C_s	Snubber capacitance	F
k_d	Coupling function for VSC	-
$k_{a,i}$	Coupling functions for cycloconverter phase legs	-
L_λ	Transformer leakage inductance	H
L	Inductance	H
R	Resistance	r
ω_0	Fundamental angular frequency	rad/s
ω_c	Carrier angular frequency	rad/s
p	Pulse number	-
M	Modulation index	-
A_{mn}, B_{mn}	Coefficients of the double Fourier series expansion	various
a_n, b_n	Coefficients of the Fourier series expansion	various
$f(t)$	Modulated function	various
δ	Duty cycle	-
α_e	Phase angle of the counter-emf	rad
φ	Load angle	rad

Content

Chapter 1
Introduction

This chapter gives a brief introduction of the background concerning the field of the thesis. After that, the objectives and the outline of the whole work are also included in the end.

1.1 Background

The switching losses of power conversion systems can be significantly reduced by the use of the proposed mutually commutated converter (MCC) topologies [1] which permit soft switching of all semiconductor valves in all operating points without any auxiliary valves. These MCCs are equipped with IGBT-based cycloconverters; however, thyristors are more suitable for such naturally commutated converters due to their inherent properties. On the other hand, some fast thyristors for high power application are available, which makes it feasible to use thyristor-based cycloconverters in a high frequency application.

The proposed space-vector oriented modulation strategy [2] which adapted for the MCCs is not suitable when thyristors are used in the cycloconverters. Several critical constrains arise due to the fact that the thyristors are not able to force the turn-off of their valves, which implies that the corresponding phase leg cannot commutate if the current reverses prior to this commutation. To solve this problem, a recently proposed current clamping MCC modulation strategy which was adapted for wind farms would be of great interest to study and analyze in a simplified three-phase power conversion system. An important topic to investigate is whether this strategy is feasible at all operating points. At the same time, the influence caused by the current clamping with regard to harmonic performance is also attractive.

In addition, it is also of interest to increase the effective switching frequency of the conversion system in order to reduce the current ripple, and consequently to reduce the total harmonic distortion. This might be achieved by the use of the cascaded MCC.

1.2 Objectives

The primary objective of this thesis is to find a feasible way which allows the thyristor-based cycloconverter to be commutated at any instant of each commutation interval. To achieve this goal, space vector modulation strategy as well as current clamping control strategy is studied and analysed.

The steps of this thesis are given in details as follows:

1. Set up a simplified power conversion system model which is studied throughout this work. Derive all equations for both the three-phase system and the degenerated single phase system.

2. Select the optimal pulse number for the studied modulation strategy by evaluating the harmonic performance.

3. Simulate both SVM strategy and current clamping control strategy with an optimal pulse number which is multiple of six (p=48) in Matlab. Compare the results regarding the current waveforms and harmonic spectrums, mainly focusing on the low order harmonic contents and THD_0.

4. Establish a cascaded topology for MCC and make a conclusion by comparing with the former results.

1.3 Outline of the thesis

Chapter 2
Firstly, the topology of the studied MCC system is described in this chapter. Subsequently, the very restrictive commutation sequence for each part of the system is introduced in details.

Chapter 3
This chapter introduces two different carrier-based modulation algorithms regarding the carrier waveform. For adapting the commutation sequence of the MCC system, space-vector oriented modulation is presented as well as its algorithm. Following that, additional constrains which has risen by the use of the thyristors in the cycloconverter are discussed. Finally, a general description of the current clamping control strategy is given.

Chapter 4
In this chapter, a simplified power conversion system is depicted by diagrams together with equivalent equations. Following that, the cascaded MCC topology is introduced in order to obtain a better harmonic performance. Furthermore, the operating points and the optimal pulse number are selected based on a mathematical analysis.

Chapter 5
As the primary purpose of this chapter, the simulation results of the conventional MCC are evaluated by supplying an optimal pulse number. Two untreatable operating conditions are shown in the subsection. In the end, the cascaded MCC is also simulated to indicate its superiority based on its higher equivalent switching frequency.

Chapter 6
This chapter summarizes the work in this thesis and brings forward future aims in this field.

Chapter 2
Mutually Commutated Converter System

The first part of this chapter provides a brief description of the MCC system from the topology point of view. Following that, the very restrictive commutation sequence is introduced in detail.

2.1 Topology of the MCC System

The topology of the studied mutually commutated converter system is illustrated in Figure 2.1. It should be mentioned that this is, however, not the only way to make the implementation in terms of the number of legs in the VSC and the cycloconverter, respectively. Other options will be represented in this section later.

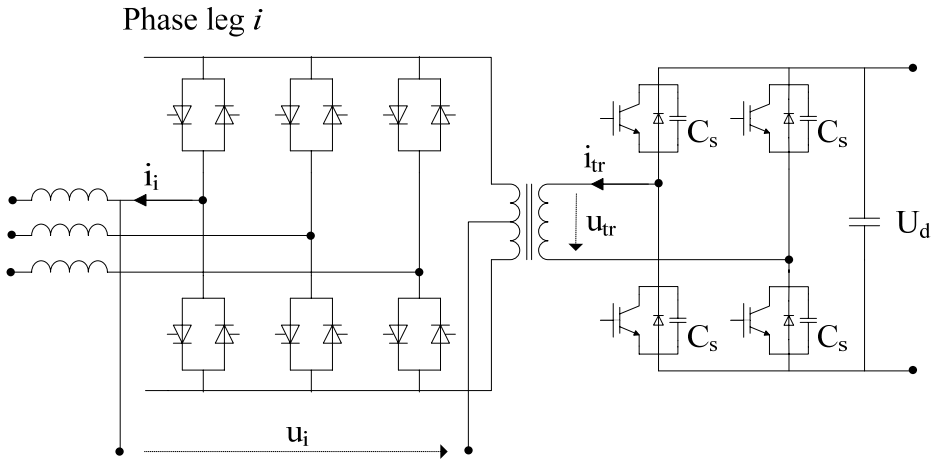

Fig 2.1 Topology of the MCC System

The indicated circuit structure in Figure 2.1 mainly has three parts: a capacitive snubbered VSC and a thyristor-based cycloconverter which are magnetically coupled by a single-phase MF transformer. Compared to the conventional AC transformer, the MF transformer operates at a much higher frequency which allows for a smaller volume and lighter weight [1]. In order to allow all the semiconductor valves to operate in the soft switching condition a compatible commutation sequence will be introduced in the subsequent sections.

As previously mentioned, there are several different solutions for designing of an MCC system in different applications with respect to the number of legs [1].

Basically, the VSC can be realized in two different topologies named as half-bridge and full-bridge. Both of the options are shown in Figure 2.2. As displayed in Figure 2.2 (a) there is only one phase leg in the half-bridge topology. The output voltage is made between the midpoint of the phase leg and the midpoint of the two equal series-

connected DC capacitors. Only two gate drive units are required which can be seen as a great advantage compare to the other option. The output voltage can assume the two levels: $\left\{-\frac{U_d}{2}, \frac{U_d}{2}\right\}$ [1].

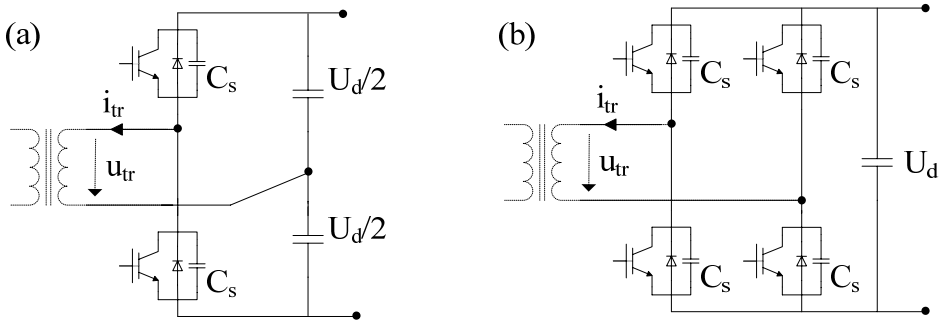

Fig 2.2 Possible VSC topologies: (a) half-bridge; (b) full-bridge [1].

The full-bridge VSC which is shown in Figure 2.2 (b) has two phase legs and the output terminal is formed between the midpoints of the legs. As a significant advantage an additional output voltage state is established while the current is freewheeling in the converter [1]. Therefore a three-level output voltage is obtainable in this case, $u_{tr} = \{-U_d, 0, U_d\}$ [1]. Moreover, this sort of connection can provide twice the output voltage of the half-bridge, given an identical DC link voltage. In reality this difference can be eliminated by the turn's ratio of the transformer, therefore it won't be a serious problem in a transformer coupled system [1].

Although there are two different solutions for the VSC topology, the main function is to convert the transformer voltage to the AC link voltage with the desired constant frequency; which is considerably higher than the grid frequency.

To meet the requirement of different systems, three options are available for the cycloconverter [1]. All possible topologies in terms of phase leg number are displayed in Figure 2.3. See figure 2.3 (a), only one phase leg is used in the simplest case where the output terminal is formed between the midpoint of this leg and the midpoint of the connected transformer winding. A three-level output is obtained in a single-phase structure which is equipped with two phase legs; see Figure 2.3 (b). In this work, the three-phase output cycloconverter is studied and adapted in a simplified power system; see Figure 2.3 (c).

A series of coupling functions are introduced in order to analyze the operation of the converter system. Throughout the analysis all voltages, currents and impedances are transferred to the VSC side, which is equivalent to assuming unity turns ratio in the transformer [1]. In order to describe how the VSC couples the DC link to the transformer at a certain instant (2.1), a function k_d is defined. The value of k_d is assumed as ±1 for a full bridge VSC when the diagonal valves are conducting and 0 when the current is circulating in the converter [1].

$$u_{tr} = k_d U_d \tag{2.1}$$

The output voltage of the cycloconverter is referred to the midpoint of the connected transformer winding. So the value of the coupling functions $k_{a,i}$ for each phase leg is assumed as {-1/2, 1/2} when the corresponding leg is connected to the lower transformer terminal and the upper transformer terminal, respectively [1]. In the following analysis, the transformer is assumed to have a unity turns ratio. Hence follows for the output phase voltages:

$$u_i = k_{a,i} u_{tr} \tag{2.2}$$

Similarly, for the transformer current, neglecting magnetizing current:

$$i_{tr} = \sum_i k_{a,i} i_i \tag{2.3}$$

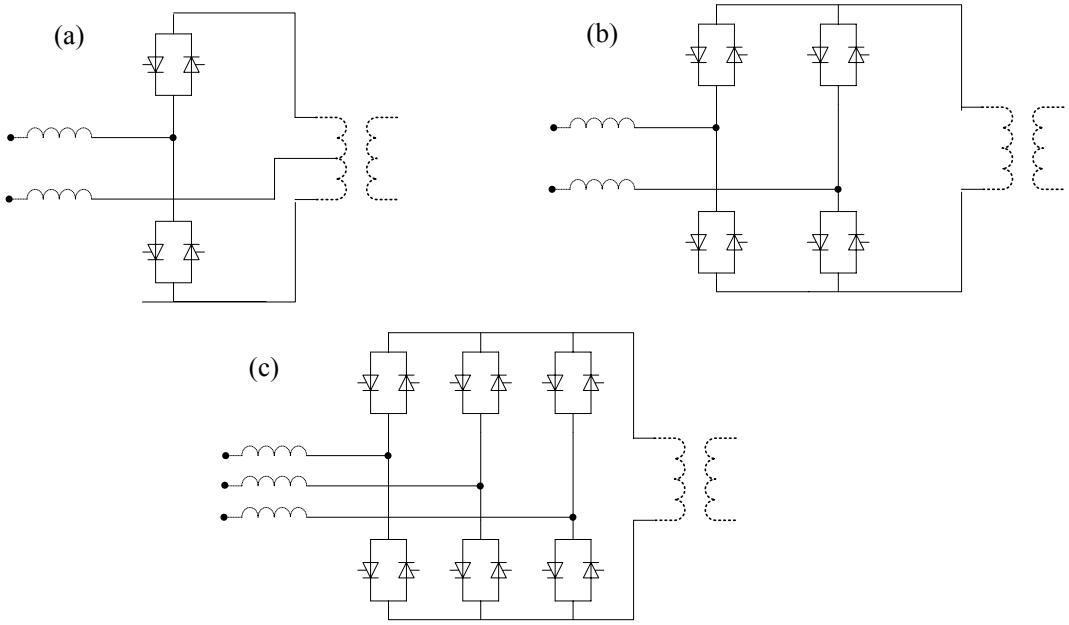

Fig 2.3 Possible cycloconverter topologies [1]

2.2 Commutation Sequence

Several important assumptions are made during every commutation cycle for the following analysis. Firstly, the voltage on the VSC side is assumed to be essentially constant, which is supplied by the DC link capacitor. Secondly, the AC side inductive filter is assumed large enough to be able to maintain the current constant in each modulation interval whereby it can be represented by a current source. Finally, the transformer is modeled by its leakage inductance L_λ and the relatively small magnetizing current is neglected in order to simplify the circuit [1]. Then, an equivalent scheme is set up during a commutation cycle and shown in Figure 2.4.

As indicated by its name the MCC converters always alternatively commutate, both natural commutation and zero-voltage commutation are enabled for the

cycloconverter and VSC, respectively [1]. The following section will give a general introduction on the commutation sequence.

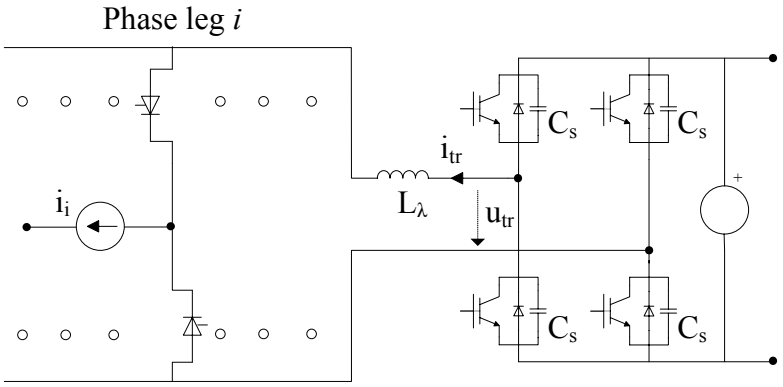

Fig 2.4 Simplified schematic for one commutation cycle [1].

2.2.1 Cycloconverter commutation

The studied cycloconverter differs from the conventional one with respect that thyristors are used instead of GTOs/IGBTs. As the only way to turn off a conducting thyristor is to let the anode current falls below the holding current, the inequation indicated in (2.4) has to be fulfilled for each phase leg in order to initial the natural commutation.

$$u_{tr} k_{a,i} i_i < 0 \tag{2.4}$$

To switch off a thyristor, the applied voltage must be opposite in direction of the anode current at the beginning of a commutation. As a result the product is negative. Figure 2.5 schematically shows an example of such a commutation.

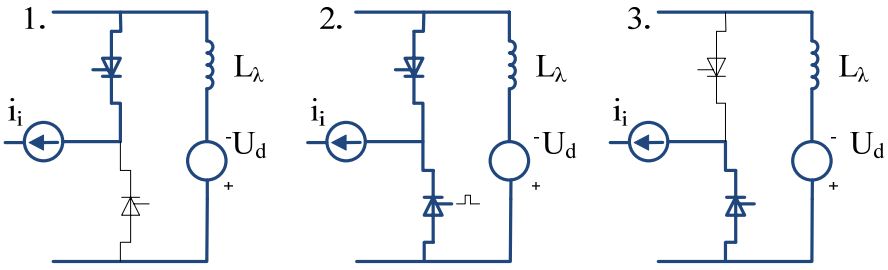

Fig 2.5 Cycloconverter phase leg natural commutation [1]

In the MCC converter, the commutation of the cycloconverter happens right after the direction of the voltage supplied by the VSC is reversed. As shown in Figure 2.5 the current of the corresponding phase leg and the voltage across the leakage inductance are opposite to each other in direction. As the negatively biased voltage is supplied across the initially conducting thyristor, the initial condition for natural commutation is established. The process is started by turning on the non-conducting thyristor in direction of the current through the phase terminal. Therefore, both of the valves are

conducting during the commutation interval until the incoming thyristor gradually takes over the current and consequently the initially conducting valve is turned off [1]. At the end of the commutation the sign of the product in Eq 2.4 changes and a new condition is valid for the next commutation.

$$u_{tr}k_{a,i}i_i > 0 \tag{2.5}$$

When all of the cycloconverter phase legs have been commutated it follows from Eqs. (2.3) and (2.5) that

$$u_{tr}i_{tr} = \sum_i u_{tr}k_{a,i}i_i = \sum_i \frac{1}{2}|u_{tr}||i_i| \tag{2.6}$$

Obviously the sign of this expression is positive which means that u_{tr} and i_{tr} are of the same sign, i.e. the instantaneous power flow is directed form the DC side to the AC side [1].

2.2.2 VSC commutation

The commutation process of the sunbbered VSC is shown in Figure 2.6 right after the cycloconverter commutation. As mentioned above, u_{tr} and i_{tr} are of the same sign which implies that the current flows through the switches instead of diodes at this stage, see Figure 2.6.

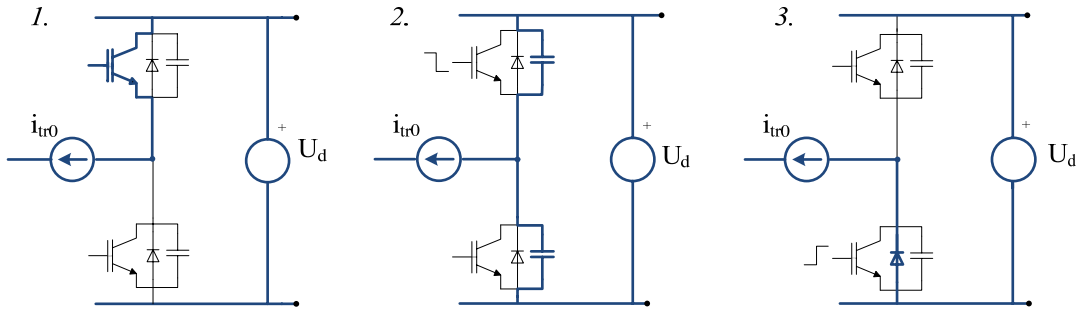

Fig. 2.6 Snubbered VSC commutation [1]

The second diagram in Figure 2.6 indicates the beginning of the process. By turning off the conducting switch, the current is diverted to the snubber capacitors. A recharging process is started until the potential of the phase terminal has fully moved to the opposite DC rail [1]. As a result, the current follows through the diode in the opposite valve. Thereby a zero-voltage and zero-current turn-on condition is satisfied for the switch connected in anti-parallel to this diode [1]. A preparation is established for the next current reversal by turning on this switch.

As described above, the cycloconverter and the VSC always commutate alternatively. Both initial commutation requirements are fulfilled at the end of each commutation.

Chapter 3
Modulation Method

Conventional modulation methods with different sorts of carrier waveforms are introduced in this chapter. Space-vector oriented modulation together with its algorithm for the MCC is described for adapting the commutation sequence. Following that, the additional constraints arisen by use of the thyristors are discussed. The current clamping control strategy is introduced at the end of this chapter.

3.1 Conventional Modulation Methods

As mentioned in the previous chapter the output of the converter can not be varied continuously but only switched between the upper and lower DC link voltage, the aim of the modulation is to create trains of switched pulses which have the same fundamental volt-second average as a target reference waveform at any instant. As the consequence of these non-sinusoidal switched pulses, unwanted harmonic components are always existed and should be minimized. Hence for all modulation methods, two basic objectives have to be achieved one after the other: the primary objective for a modulation method is to calculate the converter switch instants in order to create the desired target output voltage or current. When this most basic requirement has been satisfied, the secondary objective for a modulation method can be identified, which is to arrange the most proper switching process to minimize unwanted harmonic distortion, switching losses, or any other specified performance criterion[3].

One conventional modulation is the so called carrier-based method which compares a low-frequency target reference waveform against a high-frequency carrier waveform. The principle of this method is to switch the phase leg to the proper DC rail by judging the result of the comparison. For instance, when the reference waveform is greater than the carrier waveform, the phase leg is switched to the upper DC rail; when the carrier waveform is greater than the reference waveform, the phase leg is switched to the lower DC rail. In most cases the reference waveform is a sinusoid of an angle frequency ω_0 and the carrier is typically a triangular or sawtooth waveform of a considerably higher angle frequency ω_c. Two different sampling methods have been derived considering the practical working environment. The first one is called natural sampling method where the carrier is compared against a time-continuous sinusoidal reference which is difficult to implement in a digital modulation system as the intersection between the reference sinusoidal and the triangular or sawtooth carrier is complex to calculate [3]. In order to overcome this drawback the other sampling method is introduced and named as regular sampling method where the low-frequency reference waveforms are sampled and then held constant during each carrier interval. For a sawtooth carrier, the sampling always occurs at the beginning of each carrier cycle. Differently, there are two alternatives for a triangular carrier, symmetrical sampling and asymmetrical sampling. The former one samples the reference every carrier interval at either the positive or negative peak of the carrier;

the latter one takes the sampled reference at both the positive and negative peak of the carrier and hold it for each half carrier interval [3]. Examples of the mentioned modulation methods can be found in [1].

In order to analyze the performance of the use of different modulation methods with respect to harmonics and other specified performance criterions, the following parameters are defined.

The amount of distortion in the voltage and current is quantified by means of an index named the total harmonic distortion (THD). The THD in the voltage is defined as

$$THD = \frac{1}{V_1}\sqrt{\sum_{k=2}^{\infty} V_k^2} \tag{3.1}$$

As the amplitude of the line current is proportional to the apparent power, the THD of the line current will tend to overstate the distortion at low apparent power conditions. Therefore, the base current is chosen for normalization in this work, which gives a figure labeled THD_0.

$$THD_0 = \frac{1}{I_{base}}\sqrt{\sum_{k=2}^{\infty} I_k^2} \tag{3.2}$$

The pulse number or frequency ratio p is defined as the quotient between carrier and reference frequencies equals the number of pulses per fundamental cycle.

$$p = \frac{\omega_c}{\omega_0} \tag{3.3}$$

The quotient between the fundamental component of the peak AC output voltage and the magnitude of the phase voltage pulses is labeled as *modulation index (M)*.

$$M = \frac{\hat{U}_1}{U_q} \tag{3.4}$$

3.2 Modulation of Mutually Commutated Converter

As described in the previous section, the carrier-based modulation method could be used for such an MCC system equipped with an IGBT-based cycloconverter. Due to the constraints of the MCC commutation, the type of the sawtooth carrier waveform has to change twice [1] in each fundamental cycle of the reference waveform according to the instantaneous direction of the current which makes it more complicated compared to the proposed space vector modulation (SVM) which will be introduced in this chapter.

3.2.1 General Space Vector Modulation

The input of a converter can be assumed to be a pure DC voltage in each commutation interval and must never be shorted. On the other hand, as a basic function of converters, the output current must always be continues. Combining the requirements together, it can be assumed that the converter only has 8 distinct switching combinations, shown in Figure 3.1. In one commutation interval, the input voltage of the converter is represented by a DC voltage source and the semiconductor valves are replaced by switches for simplification. The first six combinations produce a non-zero output voltage vector and are known as non-zero switching states; the remaining combinations produce zero voltage vectors and so called zero switching states.

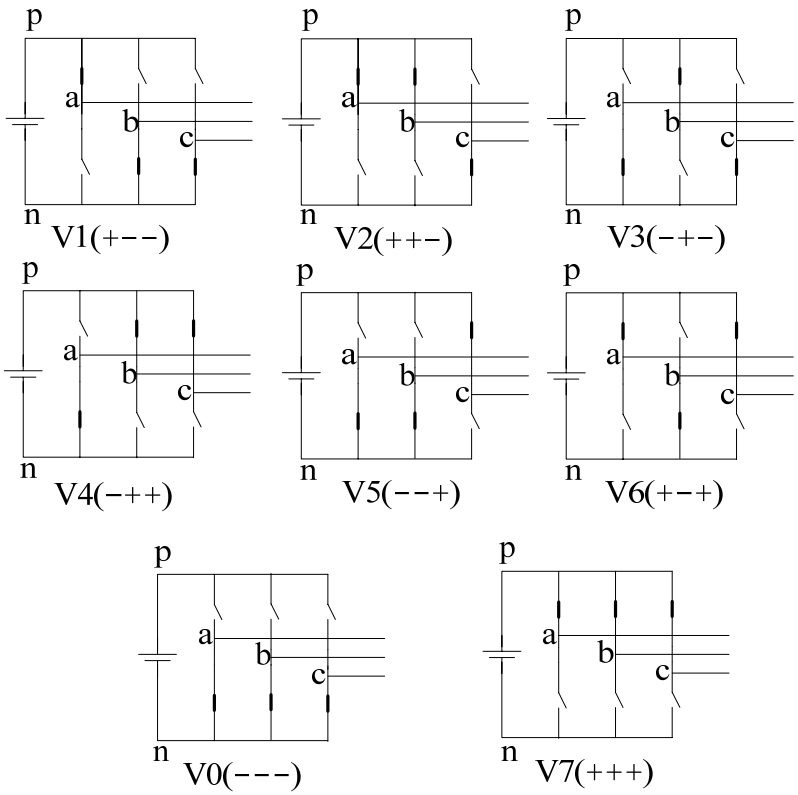

Fig 3.1 Eight switching combinations of converters in one commutation interval

The basic ideal of the space vector modulation method of three-phase system is to represent the three quantities as vectors in a two-dimensional (α, β) plane. The concept of a voltage vector is defined as

$$\bar{u} = K(u_1 + u_2 e^{j2\pi/3} + u_3 e^{-j2\pi/3}) \tag{3.5}$$

where u_1, u_2 and u_3 are the three phase voltages. Similarly a current vector is defined as

$$\bar{i} = K(i_1 + i_2 e^{j2\pi/3} + i_3 e^{-j2\pi/3}) \tag{3.6}$$

where i_1, i_2 and i_3 are the three phase currents.

In order to obtain an amplitude-invariant transformation the constant K is set as 2/3 [1].

Using this definition, the output voltage of the eight switching combinations can be transferred into the voltage vector and *are called base vectors*. The non-zero switching states give the active base vectors ($\overline{V_1}$ through $\overline{V_6}$) and the zero switching states give the zero vectors ($\overline{V_0}$ and $\overline{V_7}$). The six active base vectors are symmetrically distributed in the α β plan and a regular hexagon is formed by their tips, see Figure 3.2

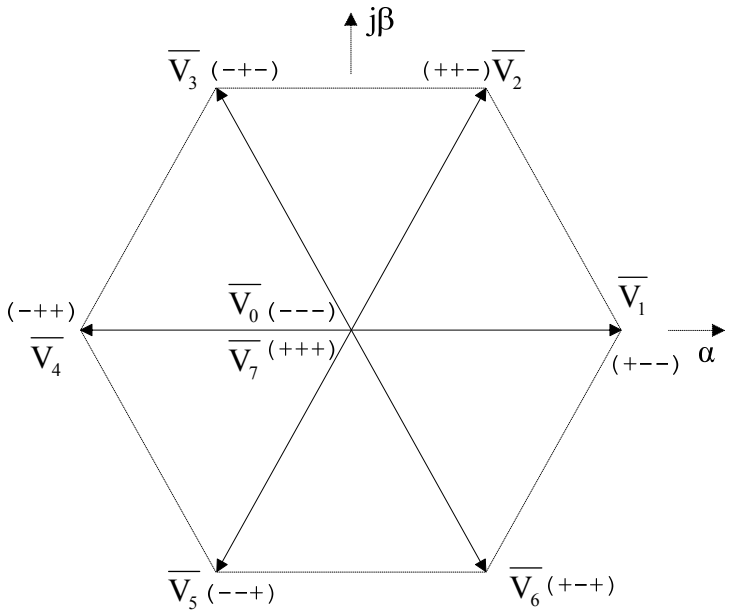

Fig 3.2 Voltage base vectors in α β plan

It can be seen in Figure 3.2 that the amplitude is zero when these two zero vectors are overlapped and located in origin. An expression can be made in order to describe the active vectors in the two-dimensional plan [2].

$$\overline{V_p} = \frac{4}{3} U_q e^{j(p-1)\pi/3} \text{ for p=1,…,6.} \tag{3.7}$$

where U_q is the effective DC link voltage and the q represents the corresponding switching state.

In the same manner, the desired output voltage could be represented by an equivalent vector rotating in the counter clock wise direction and expressed by real and imaginary parts: $\overline{u}^* = u_\alpha^* + j u_\beta^*$. Since the output voltages of the three phase legs are discrete and switched between positive and negative DC link voltages, the essence of the output pattern of the cycloconverter is a series of switching combinations which means the instantaneous output voltage vector is always one of the voltage base

vectors. From this point of view the desired output voltage vector may be synthesized by several voltage base vectors and their duty cycles during the modulation interval. In normal modulations, the sequence of one modulation interval is always initiated by one of the zero vectors and ended by the other [2]. Two active vectors are imposed between the zero vectors and adjacent to the reference vector. An example is made in Figure 3.3 where the reference vector is located between $\overline{V_1}$ and $\overline{V_2}$.

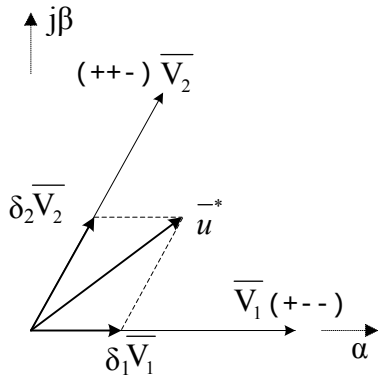

Fig 3.3 Synthesis of the desired output voltage vector

As indicated in the Figure 3.3 δ_1 and δ_2 are the corresponding duty cycles of $\overline{V_1}$ and $\overline{V_2}$, respectively. The duty cycles are defined as

$$\delta_i = T_i / T_s \tag{3.8}$$

where T_s is the switching interval and T_i is functioning time of the concerned base vector.

By solving (3.9) the duty cycles of the imposed active vectors can be determined easily.

$$\delta_1 \overline{V}_{p_1} + \delta_2 \overline{V}_{p_2} = \overline{u}^* \tag{3.9}$$

where $\overline{V}_{p_1}$ and $\overline{V}_{p_2}$ represent the active vectors which are adjacent to the sampled reference vector in the concerned modulation interval.

The total duty cycle of the zero vectors is the remains of the modulation interval as

$$\delta_z = 1 - \delta_1 - \delta_2 \tag{3.10}$$

The duty cycles δ_1, δ_2 and δ_z are uniquely determined from (3.9) and (3.10), therefore the remaining degrees of freedom are the sequence of the vectors and the distribution of the total zero vector duty cycle [1].

3.2.2 Principle of the Space Vector Modulation for MCC

The modulation of the mutually commutated converter has several constraints compared with the conventional ones due to the requirement of soft switching commutation.

Firstly, due to the constant frequency of the VSC commutation one of the flanks of each pulse will be always be placed at equidistant points of time. The other flank is determined by the cycloconverter commutation and may be arbitrarily placed within the modulation interval [1].

Secondly, the sign of each phase voltage and the corresponding phase current have to be opposite to each other at the beginning of the cycloconverter commutation in order to fulfill the conditions for natural commutation.

Finally, as the commutation of the VSC gives an opposite polarity for all phase voltages at the beginning of the modulation interval, the sign of each phase voltage and the corresponding phase current should be identical at the end of the commutation to allow for the next commutation.

The mentioned constraints can be better understood by a space vector approach. The current space vector has been defined in (3.6) in the α-β plane and rotating in the counter clock wise direction. The covered area is split up six regions depending on the sign of each phase current, see Figure 3.4.

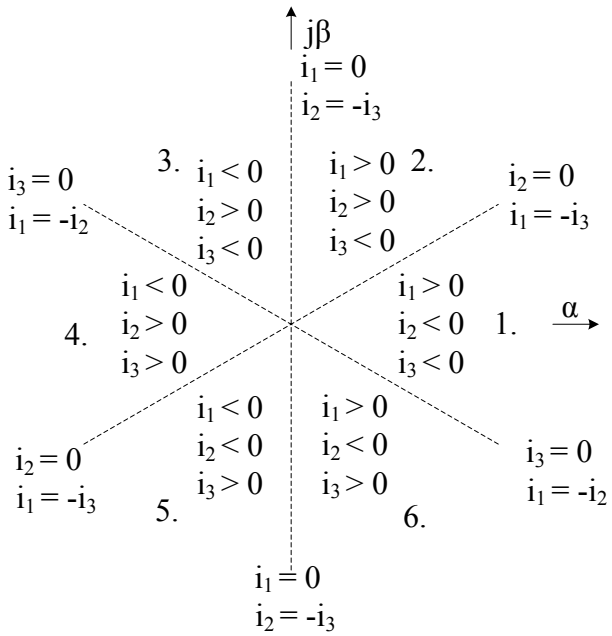

Fig 3.4 Current direction regions [1]

Note that the boundaries of the current sectors are shifted π/6 compared to the case of the voltage vector. When the current vector crosses the boundary which is located between two adjacent sectors, the direction of the phase current only reverses in one phase leg.

By recalling Figure 3.2 the requirement of natural commutation for a certain current vector will be fulfilled when the initial voltage base vector is opposite to the current vector located sector. As previously discussed, the commutation sequence will be ended up by an active voltage vector located in this current sector for continues natural commutations. Furthermore, one phase leg can only be commutated once in each modulation interval, which implies that there are six four-vector voltage sequences for a certain current vector [2], shown in Figure 3.5. Assume that the current vector is located in sector 1.

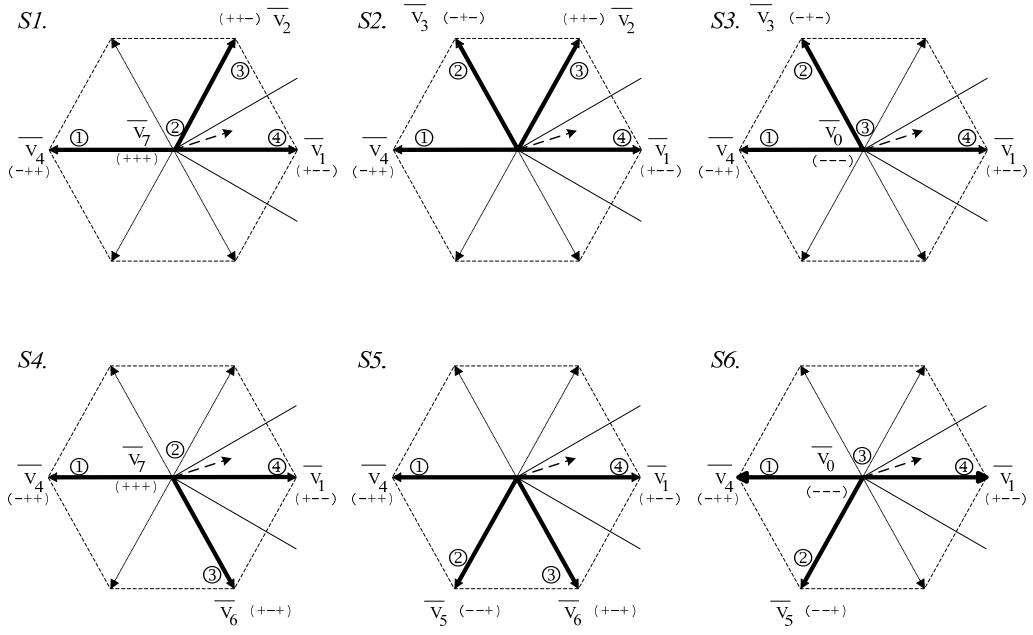

Fig 3.5 Possible voltage base vector sequences with the current vector located in sector1.

For other cases where the current vector is not located in sector 1, the possible voltage base vector sequences are similar to the case shown in Figure 3.5. A same voltage base vector location can be obtained by shifting the hexagon with respect to the new current sector [2]. In practice, either the first or the last voltage base vector is moved to the very beginning or end of the modulation interval and suppressed with the second or the third base vector, respectively. Therefore, the number of the base vectors is reduced from four to three. This method is attractive as it not only simplifies the implementation but also avoids the opposition of the voltage vectors in each modulation interval which gives a reduction in the current ripple [2].

3.2.3 Space-Vector Oriented Modulation for MCC

When the reference voltage vector is taken into consideration, the selection of the optimum vector sequence becomes a problem. It is solved by the space-vector oriented modulation which is derived in [2] and described briefly in this work.

In this method all current vectors are transferred to the equivalent first sector by shifting the hexagon in order to simplify the process. The reference voltage is shifted into a new system labeled as α'β'-system by (3.11) with respect to the current vector [2].

$$\overline{u}^{*'} = \overline{u}^{*} e^{-j(k-1)\pi/3} \tag{3.11}$$

where *k* stands for the region where current located.

The α'β'-system is established and divided into twelve regions as shown in Figure 3.6. When the load angle of the vector is either between π/3 and 2π/3 or between -2π/3 and -π/3, the vector located region will be given by (3.12) [2]. The inner sectors (B1, C1, F1 and G1) are chosen when the inequality is true [2].

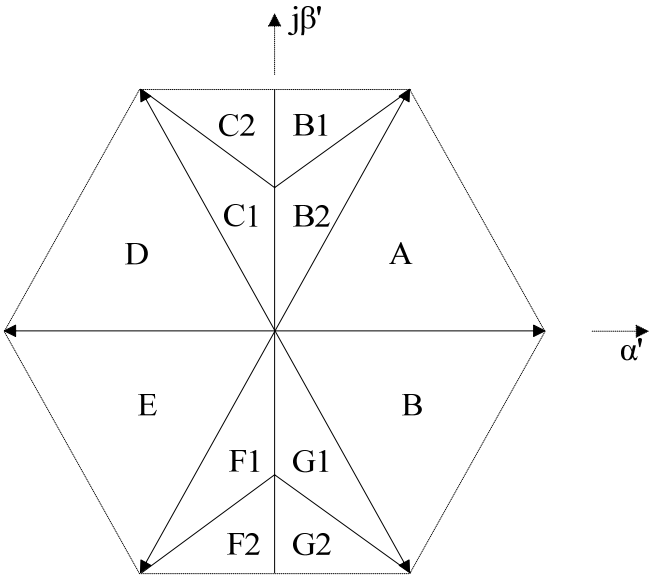

Fig 3.6 Voltage regions in the α'β'-plane [2]

$$\sqrt{3}\left|u^{*}_{\beta'}\right| - \left|u^{*}_{\alpha'}\right| < \frac{2}{3}U_d \tag{3.12}$$

With the preparations above, the optimum base vector sequence can be decided by TABLE 1 in α'β'-system and the duty cycle can be obtained by solving (3.13) [2].

TABLE 1
BASE VECTOR SEQUENCE IN α'β'-SYSTEM [2]

$\overline{u}^{*'}$ region → Base vector (i) ↓	A	B1	B2	C1	C2	D	E	F1	F2	G1	G2	H
1	7	4	4	3	3	4	4	5	5	4	4	7
2	2	7	3	0	2	3	5	0	6	7	5	6
3	1	2	2	1	1	0	0	1	1	6	6	1

$$\begin{pmatrix} V_{p_1,\alpha'} & V_{p_2,\alpha'} & V_{p_3,\alpha'} \\ V_{p_1,\beta'} & V_{p_2,\beta'} & V_{p_3,\beta'} \\ 1 & 1 & 1 \end{pmatrix} \begin{pmatrix} \delta_1 \\ \delta_2 \\ \delta_3 \end{pmatrix} = \begin{pmatrix} u^*_{\alpha'} \\ u^*_{\beta'} \\ 1 \end{pmatrix} \tag{3.13}$$

So far, both the commutation sequence and the duty cycle for each base vector are solved in the transferred system; therefore an inverse transformation is needed to offer the proper sequence with the aid of the TABLE 2.

TABLE 2
CONVERSION OF THE BASED VECTOR
FROM THE α'β'-SYSTEM TO THE αβ-SYSTEM [2]

α'β'-base vector → Current region (k) ↓	0	1	2	3	4	5	6	7
1	0	1	2	3	4	5	6	7
2	7	2	3	4	5	6	1	0
3	0	3	4	5	6	1	2	7
4	7	4	5	6	1	2	3	0
5	0	5	6	1	2	3	4	7
6	7	6	1	2	3	4	5	0

3.3 Additional Difficulties for MCC without Cycloconverter Turn-off Capability

The proposed space-vector oriented modulation method samples the output currents ahead of the beginning of each commutation interval and assumes that the current vector is not leaving the initial sector during this period. As a matter of fact, the current vector is rotating continuously and may oscillate around the boundary of a current sector, therefore, the sampled vector probably moves to the neighboring sector during the commutation. As previously described, the sign of each phase voltage has to be opposite to the sign of the corresponding line current in order to allow the natured commutation. If one of the line currents has changed sign during a modulation interval, the cycloconverter equipped with IGBTs is able to force the turn-off of its valves, which allows the commutation scheme to maintain the desired pulse pattern regardless of a probable zero-crossing of the line currents. In this case an additional phase leg commutation is required at the end of this modulation interval in order to establish the conditions for continuous natural commutations [4].

But regarding the thyristor-based cycloconverters, their valves lack turn-off capability and, hence, can not turn off their valves without the complex and expensive external circuits. For this reason, after a current sign reversal, the condition for commutating the corresponding phase leg will not be re-established anymore and one of the directions in the voltage hexagon will be inhibited.

Therefore, it is important to make a correct decision when a line current is approaching zero and the commutation of the corresponding phase leg is still not

decided. Generally, two feasible options are available. Firstly, a commutation can be made just before the zero-crossing by breaking the desired duty cycle. Consequently, an additional commutation may be needed at the end of the interval for the following commutation if the line current still changes sign. In the other case, the commutation of the corresponding phase leg can be either delayed or avoided by re-arranging the base vector sequence. Although it probably can not provide the desired pulse pattern, the additional phase leg commutation can be avoided.

As another constraint arises from the thyristor, a reverse voltage has to be maintained across it during the turn-off time t_q. If a biased voltage is supplied to a thyristor during this interval, an unintentional turning-on will happen and the thyristor cannot be turned off in this commutation interval anymore which results in an undesired pulse pattern. Therefore the duty cycle for each base vector has to be longer than the minimum interval t_q.

3.4 Description of the Current Clamping Control Strategy

As mentioned in the previous section, due to the limited controllability, a cycloconverter equipped with thyristors may not maintain the desired base vector sequence if the current vector goes into another sector during the commutation. Therefore, a feasible solution is needed whenever the current vector undesirably leaves the initial sector. A new modulation strategy is proposed by Stephan Meier in [4], labeled as *current clamping control strategy*. The basic idea of this strategy is *to stop the gate pulses in the conducting thyristor valve during a certain dead-time whenever the current in the corresponding phase leg becomes zero [4]*. The gate pulses will be re-supplied after the dead-time and the currents will finally reverse at a desired instant.

According to the space vector modulation method introduced in Section 3.2.3, the base vector sequences and their duty cycles can be determined. By modeling a simplified three-phase power conversion system (see Section 4.1 for further details), the current vector trajectory can be predicted for the calculated base vector sequence. With the help of the predictor, the dead time can be precisely calculated and a new base vector sequence can be determined if it is necessary before the beginning of every modulation interval.

The process of the current clamping control strategy can be concluded as two parts. Firstly, predict the current trajectory with the sampled current vector and the desired voltage vector. The cycloconverter is treated as the one equipped with IGBT so that it has the turn-off capability in the first process. With this assumption it is possible to use the space vector oriented modulation for MCC in order to determine the base vector sequences and the corresponding duty cycles. The current trajectory can be obtained by applying the calculated results on the target model.

Secondly, determine the exact clamping instants and the new base vector sequence. When the current is leaving the initial sector, which implies that the sign of one of the line currents will reverse, the predictor must determine whether the current clamping

is necessary. Basically, according to the comparison between the initial and the last current vectors referred to the current sector, two situations are obtained (see E1 and E2 in Figure 3.7). E1 is the case where the current trajectory is only temporarily leaving the initial current sector during a modulation interval. In such cases the current reversal always happen before the commutation of the corresponding phase leg and has to be avoided. As shown in Figure 3.7, the commutation of the phase leg c_3 is delayed until the current trajectory goes back into the initial sector. The predicted base vector sequence is 3→0→1→6 as shown in the upper color bar of E1, the corresponding duty cycles are represented by the length of the bars. As a matter of fact, as the first base vector 3 is suppressed by the second base vector 0 at the beginning of the modulation interval, the effect of base vector 3 can be neglected. Similarly, all the bars given in white denote that the concerned base vector is suppressed by the neighboring one. The desired sequence is maintained in this sort of cases with modified duty cycles when the current clamping control strategy is valid. See the lower color bar of E1, the first base vector is not influenced by the current clamping while the dead time injected between the second and the last duty cycle, represented by the yellow bar. During the dead time, the current of the corresponding phase leg is clamped to zero and as a consequence the current vector is moving along the boundary. This is done by stopping the gate pulses to the anti-parallel thyristor in the conducting valve of the corresponding phase leg.

E2, E3 and E4 in Figure 3.7 are the cases where the current trajectory will finally move into another current sector at the end of the commutation interval. In such cases the current clamping control strategy is not always needed, a judgment has to be made before the beginning of the prediction. If the sign of the line current is going to reverse and the corresponding phase leg is still waiting for the commutation within the desired modulation interval, the current clamping is not avoidable in order to refrain from this improper commutation, see E2 and E3 in Figure 3.7. Contrarily, if the commutation of the corresponding phase leg is only needed before an additional commutation at the end of this modulation interval, the current clamping is not necessary anymore and the soft switching commutation is still available for any phase legs just by canceling this improper commutation, see E4 in Figure 3.7. This is the favorable case as the additional phase leg commutation can be avoided without the calculation of the dead time.

The desired voltage base vector sequence in a conventional manner is not suitable for the case E2 as the phase leg in which the current is changing sign is not commutating at all. As a consequence, the determination of the dead time in this case is more complex than the case in E1 due to the fact that it is not only settled by the current reversal instance but also determined by the new voltage sequence. The easy way to determine the dead time is based on ending up the current vector trajectory at the same point as in the conventional manner. The current in the corresponding phase leg is clamped when it is approaching zero and released at the instant which can let it coincide with the desired end point at the end of the commutation interval. See the color bar of E2 in Figure 3.7, in this way the commutation of C2 as well as the additional commutation at the end of the modulation interval is avoided.

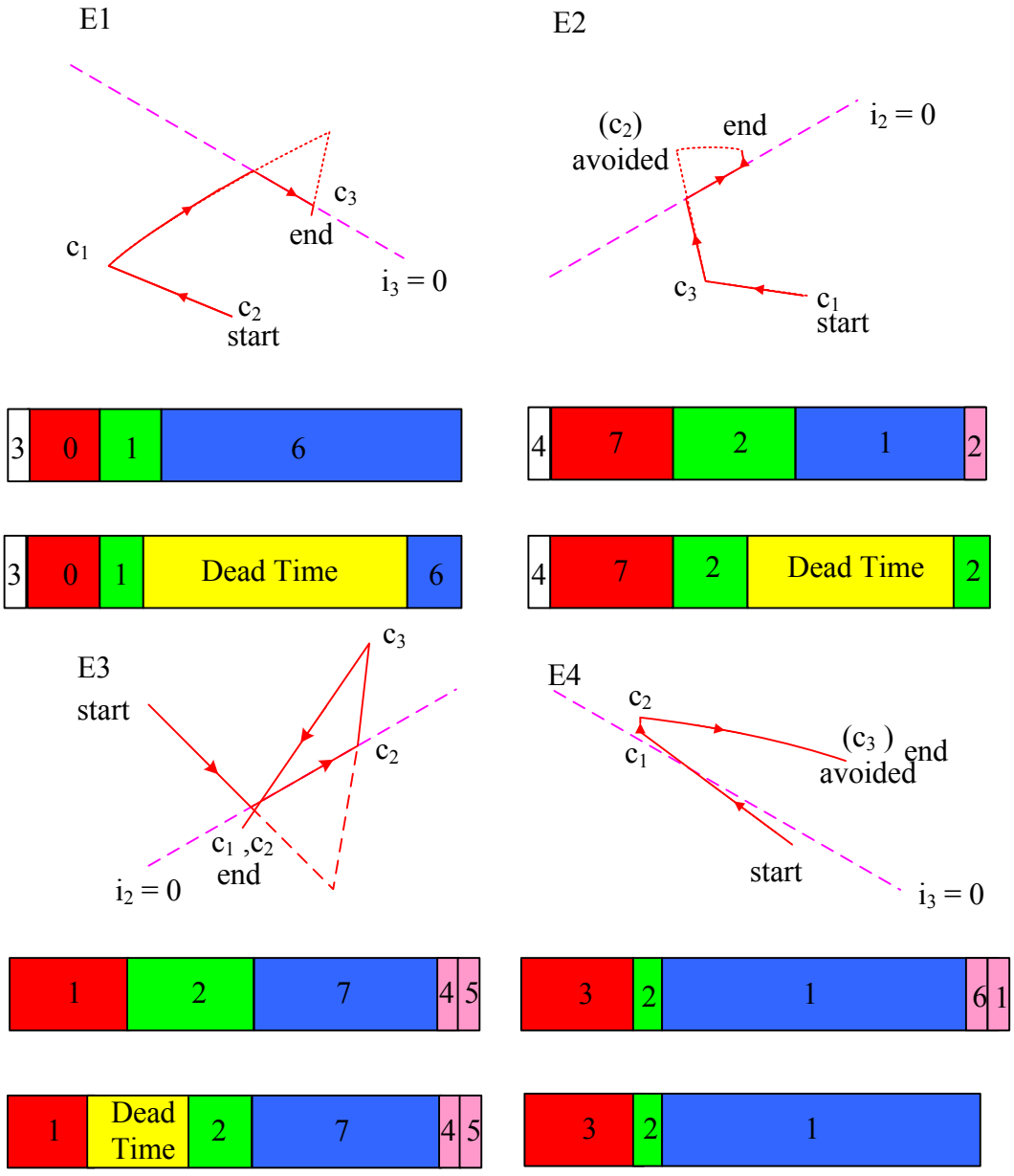

Fig 3.7 Examples of current trajectories with current clamping control strategy, base vector sequences and their corresponding duty cycles.

It should be noticed that in case E3, the current trajectory temporarily leave the initial current sector in the front part of the commutation interval and is actually required to move to another sector in the end. It can be treated as case E1 with one additional commutation at the end of this modulation interval. In this special case, the corresponding phase leg C2 is commutated twice in the modulation interval. When the second commutation of C2 occurs, the base vector 4 is functioning and $i_2<0$, which implies that the condition $u_2i_2<0$ is still fulfilled.

It should be noticed that the four cases discussed in this section are only some common and basic cases, more complex current trajectories may occur. For example,

in some high current ripple cases, the current vector trajectory may temporarily cross more than one sector in a commutation interval and also can be solved similarly as in example E1.

Chapter 4
Power conversion system Model and Cascaded MCC

Firstly, this chapter gives a brief description of the power conversion system model together with its equivalent equations. To increase the equivalent switching frequency, cascaded MCC is introduced in the subsection. Operating points and the optimal pulse number are selected in the end.

4.1 Simplified three-phase power conversion system model

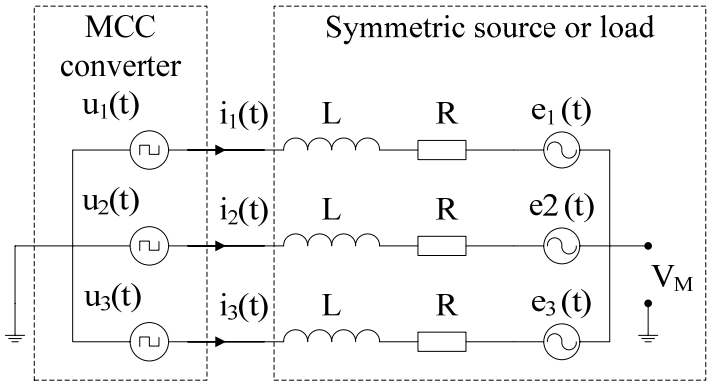

Fig 4.1 Three-phase power conversion system of which load or source with unconnected midpoint connected to a MCC converter

Figure 4.1 is a three-phase power conversion system of which the right part is a three phase load or source with unconnected midpoint connected to a MCC converter. The load or source side is presented by counter-emf, which is assumed robust and pure sinusoidal. The value of the inductance L, resistance R and the amplitude of the counter-EMF are 0.2 p.u., 0.01 p.u. and 1 p.u., respectively.

In time domain the equation for each phase is given in Eq 4.1.

$$u_i - L\frac{di_i}{dt} - Ri_i - e_i - v_M = 0 \text{ for } i=1,2,3 \tag{4.1}$$

where the v_M is the potential of the unconnected midpoint M and given in Eq 4.2

$$v_M = \frac{1}{3}\sum_i u_i \qquad \text{for } i=1,2,3 \tag{4.2}$$

The counter-EMF is assumed pure sinusoidal and defined by (Eq 4.3) for each phase leg.

$$\begin{aligned} e_1 &= E\cos(\omega_0 t + \alpha_e) \\ e_2 &= E\cos(\omega_0 t + \alpha_e - \frac{2\pi}{3}) \\ e_3 &= E\cos(\omega_0 t + \alpha_e + \frac{2\pi}{3}) \end{aligned} \tag{4.3}$$

As the SVM is used in the simulation, all parameters should be represented in terms of space vector, this is done by multiplying (4.1) by1, $e^{j2\pi/3}$ and $e^{-j2\pi/3}$ and add them together, see Eq 4.4.

$$\bar{u} - L\frac{d\bar{i}}{dt} - R\bar{i} - \bar{e} = 0 \tag{4.4}$$

where $\bar{e} = Ee^{j(\omega_0 t + \alpha_e)}$.

In the simulation, the initial current vector is set according to different operating points listed in Table3. The phase angle of the counter-EMF α_e and the amplitude of the desired voltage vector U can be calculated by solving the Eq 4.5 in steady-state.

$$\begin{aligned} \alpha_e &= \arcsin\left(\frac{I}{E}\left[R\sin\varphi - \omega_0 L\cos\varphi\right]\right) \\ U &= I(R\cos\varphi + \omega_0 L\sin\varphi) + E\cos\alpha_e \end{aligned} \tag{4.5}$$

As mentioned in the section 3.4, the corresponding phase leg is isolated from the grid when the current is clamped to zero which means that the original three-phase system degenerates into a single phase system as well as the voltage equations during this stage, for instance the phase leg 2 is isolated, and the equivalent topology is shown in Figure 4.2. Considering $i_1 = -i_3$ and $i_2 = 0$ the degenerated equations in the time domain are given in Eq 4.6.

$$(u_1 - u_3) - 2L\frac{di_1}{dt} - 2Ri_1 - (e_1 - e_3) = 0 \tag{4.6}$$

thus

$$\frac{di_1}{dt} = \frac{1}{2L}\left(\left[u_1 - u_3\right] - 2Ri_1 - \left[e_1 - e_3\right]\right) \tag{4.7}$$

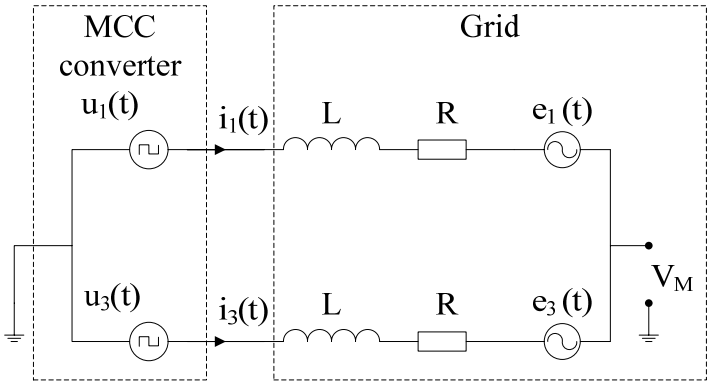

Fig 4.2 The degenerated system.

4.2 Cascaded MCC

By use of the cascaded topologies shown in Figure 4.3 the effective pulse number can be doubled without increasing the switching frequency. This elevated pulse number will give a lower current ripple which turns into a better harmonic performance. The upper and the lower topologies correspond to the full-bridge and the half-bridge cascaded MCC, respectively. As there is no principle difference between these two topologies with respect to the commutation process, the full-bridge cascaded MCC is used in the following analysis. It should be mentioned that in order to obtain an identical output current, the value of the phase inductance of the full-bridge topology is twice as high of the one of the half-bridge topology refers to a same DC link voltage. Similarly, when the phase inductance of the full-bridge cascaded MCC is twice much of the one of a single-bridge MCC, the amplitude of the fundamental output currents will be the same by supplying an identical DC link voltage.

As shown in Figure 4.3, the lower output square wave voltage of the VSC is shifted a quarter cycle compared to the upper case. As a consequence, the sampling of the reference voltage of the lower cycloconverter is also accordingly shifted, shown in Figure 4.4. Therefore a doubled effective pulse number of the cascaded MCC is obtained compared to each single bridge MCC. In the simulation, the operation of each MCC bridge is assumed independent to each other. The line currents of each bridge are combined together as the output line current of the cascaded MCC.

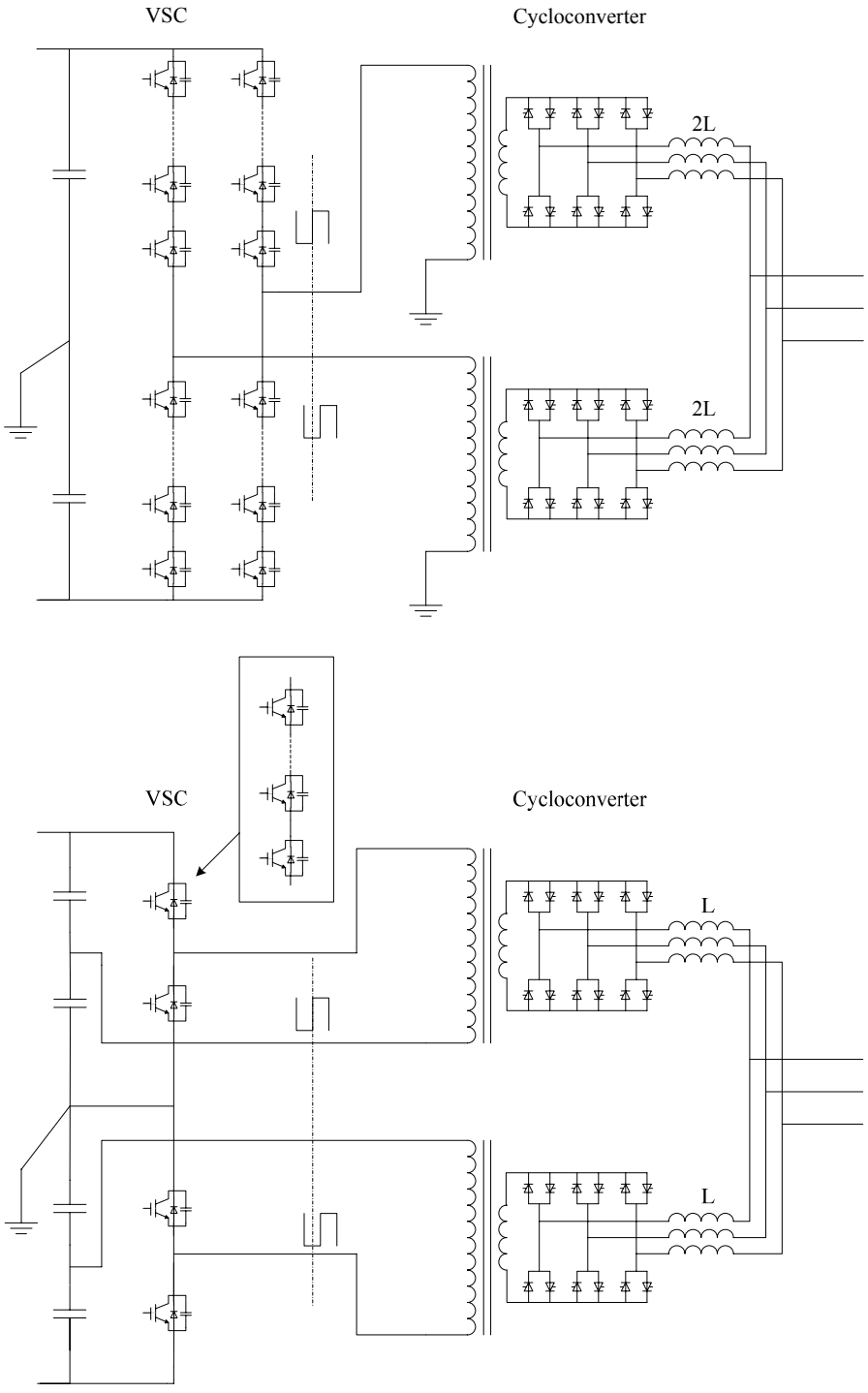

Fig 4.3 Two options for the cascaded topology

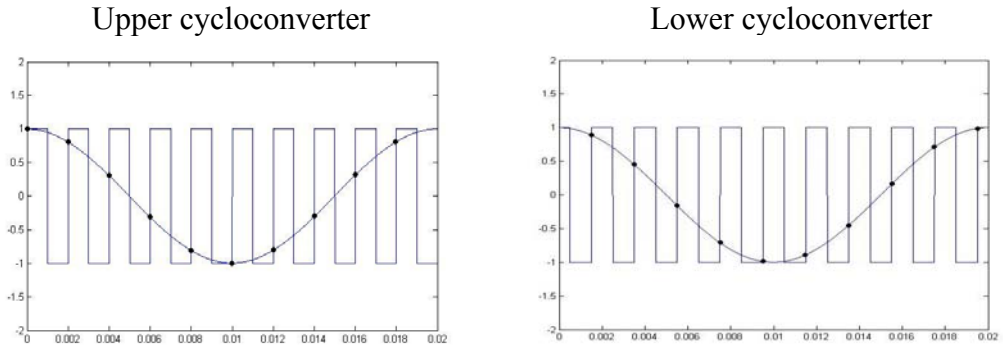

Fig 4.4 Sampling instances of upper and lower cycloconverters.

4.3 Operating Points and Pulse number

4.3.1 Operating Points

A MCC converter should be able to control both active and reactive power. From this point of view, a number of operating points have been chosen according to P and Q, shown in Table 3. The ideal amplitude of the current vector and the load angle in steady-state can be obtained by solving (4.8) which is derived according to the circuit shown in Figure 4.5; both of them are essential parameters for simulating. The parameters are given in p.u. values.

The corresponding phase leg is isolated when the current clamping strategy is functioning. This will give a floating output phase voltage. Therefore the output phase current is selected to analyze rather than the output pulse pattern. Moreover, the operating point where P=Q=0 is neglected as the output phase current is zero.

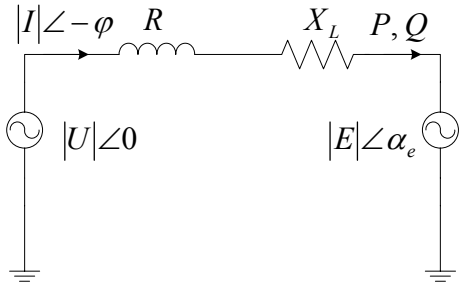

Fig 4.5 One phase of the simulated system

$$\begin{cases} -P &= \dfrac{3EU\sin\alpha_e}{X_L} \\ -Q &= \dfrac{3E(E-U\cos\alpha_e)}{X_L} \\ \sin\alpha_e &= \dfrac{I}{E}\left(R\sin\varphi - X_L\cos\varphi\right) \\ U &= I\left(R\cos\varphi + X_L\sin\varphi\right) + E\cos\alpha_e \end{cases} \tag{4.8}$$

Table 3 Operating points of the conventional MCC

Operating point	*M*	*I_0 (p.u.)*	*Φ (rad)*	*P (p.u.)*	*Q (p.u.)*
1	1.003	0.7444	0.5380	1	0.5
2	0.995	0.3329	1.5208	0	0.5
3	1.003	0.7444	2.5036	-1	0.5
4	0.941	0.6658	2.9591	-1	0
5	0.88	0.7444	-2.8698	-1	-0.5
6	0.87	0.3329	-1.6208	0	-0.5
7	0.88	0.7444	-0.3717	1	-0.5
8	0.941	0.6658	0.0826	1	0

Similarly, the operating points of each bridge of the cascaded MCC are listed in Table 4. As discussed in section 4.2, the phase inductance is 0.4 p.u. in this case.

Table 4 Operating points of each bridge of the cascaded MCC

Operating point	*M*	*I_0 (p.u.)*	*Φ (rad)*	*P (p.u.)*	*Q (p.u.)*
1	1.003	0.3722	0.5380	0.5	0.25
2	0.995	0.1665	1.5208	0	0.25
3	1.003	0.3722	2.5036	-0.5	0.25
4	0.941	0.3329	2.9591	-0.5	0
5	0.88	0.3722	-2.8698	-0.5	-0.25
6	0.87	0.1665	-1.6208	0	-0.25
7	0.88	0.3722	-0.3717	0.5	-0.25
8	0.941	0.3329	0.0826	0.5	0

4.3.2 Selection of the pulse number

Since it is quite complex to determine the harmonic components of a PWM switched phase leg output, a method by means of an analytical solution called *double Fourier series expansion* is introduced. This method was first developed by Bowes and Bird to adapt the modulated converter systems and was originally developed for commutation systems. The analysis process assumes the modulated waveform is composed by two time variables *x (t)* and *y (t)*, shown as below.

$$x(t) = \omega_c t + \theta_c \tag{4.9}$$

$$y(t) = \omega_0 t + \theta_0 \tag{4.10}$$

These variables can be considered as representing the high-frequency carrier waveform and the low-frequency reference waveform respectively. And a modulated waveform *f (t)* can be expressed as *f{x (t), y (t)}*. A double Fourier series expansion can be developed for a double variable controlled waveform from a traditional Fourier series expansion [3], as

$$\begin{aligned} f(t) = \frac{A_{00}}{2} &+ \sum_{n=1}^{\infty}\left[A_{0n}\cos(n\left[\omega_0 t+\theta_0\right]) + B_{0n}\sin(n\left[\omega_0 t+\theta_0\right])\right] \\ &+ \sum_{m=1}^{\infty}\left[A_{m0}\cos(m\left[\omega_c t+\theta_c\right]) + B_{m0}\sin(m\left[\omega_c t+\theta_c\right])\right] \\ &+ \sum_{m=1}^{\infty}\sum_{\substack{n=-\infty \\ (n\neq 0)}}^{\infty}\begin{bmatrix} A_{mn}\cos(m\left[\omega_c t+\theta_c\right]+n\left[\omega_0 t+\theta_0\right]) \\ + B_{mn}\sin(m\left[\omega_c t+\theta_c\right]+n\left[\omega_0 t+\theta_0\right]) \end{bmatrix} \end{aligned} \tag{4.11}$$

where

$$A_{mn} = \frac{1}{2\pi^2}\int_{-\pi}^{\pi}\int_{-\pi}^{\pi} f(x,y)\cos(mx+ny)\,dx\,dy \tag{4.12}$$

$$B_{mn} = \frac{1}{2\pi^2}\int_{-\pi}^{\pi}\int_{-\pi}^{\pi} f(x,y)\sin(mx+ny)\,dx\,dy \tag{4.13}$$

The first term where *m=n=0* of Eq 4.11 corresponds the DC offset component of the signal. The first summation term where the *m=0*, defines the harmonic at integer multiples of the desired output waveform frequency. Obviously, the fundamental is obtained when n=1. Low-order harmonics around the fundamental output exist in this term which should be minimized, and the harmonics in this term are called *baseband* harmonics. The second summation term where *n=0,* defines the harmonic at integer multiples of the carrier waveform frequency which are relatively high-frequency components. Finally, the double summation term where $m, n \neq 0$, corresponds the groups around the carrier harmonic frequencies. These are referred to *sideband* harmonics.

According to [1], the only harmonics that will exist in the phase voltage of a MCC, apart from the fundamental, are odd sidebands harmonics ($A_{mn}=B_{mn}=0$, when *n* is even). Moreover, the order of all sideband harmonics can be represented as $k=mp+n$, where *p* is the pulse number. This implies that all even harmonics in the output phase voltage can be eliminated by choosing an even pulse number.

On the other hand, if the output phase voltages are symmetrically shifted by 2T/3 and periodical with a cycle T, the phase voltages $u_1(t)$, $u_2(t)$ and $u_3(t)$ fulfill the following expression

$$u_1(t)= u_2(t+2T/3)= u_3(t-2T/3) \tag{4.14}$$

Decomposing these three waveforms by the Fourier series expressions, all components with the same triplen *h* are identical with respect to each other in the

expressions [3]. Thus all components at integer multiples of three times the fundamental frequency will be absent in the line-to-line voltages. For the case in an MCC system, the expression (4.14) can be fulfilled if the reference voltage in each phase leg is equally sampled within each cycle and this is only possible when the pulse number is an integer multiple of three [1].

When these two analyses are taken into account together, it becomes clear that the optimum pulse number should be a multiple of six with respect to the harmonic performance. In the case of MCC modulation, neither even nor triplen harmonic will present in the line-to-line voltages. However all non-triplen odd harmonics may still exist in the line-to-line voltages such as the ones at orders $k = 6r-1$ and $k = 6r+1$ where $r = 1, 2, 3$ etc.

Chapter 5
Solution Analysis

As the main purpose of this chapter, the simulation results of the conventional MCC with an optimal pulse number are evaluated. Following that, two untreatable operating conditions are listed. Finally, the improvement made by the cascaded topology is shown.

5.1 Evaluation of the modulation strategy

The current vector trajectories and the line current waveforms at steady-state for both conventional SVM for MCC and the current clamping strategy are shown in Figure 5.1 for operating point 8. For the reason discussed in section 4.3.2 the pulse number is chosen as 48. Comparing the current trajectories for the two different modulation strategies, it can be observed that they only differ around the boundary-crossings. In the case of current clamping MCC SVM the current vector goes along the corresponding boundary instead of temporarily leaving the initial sector.

Looking closer at the line current waveforms, the zero-crossings are avoided and the current is clamped at zero during the dead time in the case for the current clamping strategy. As a consequence of this alternation of the waveform, the harmonic performances for both cases are different in several ways, see Figure 5.2. In this specific case, the fundamental content of the current clamping MCC SVM is increased a little bit compared to the case of MCC SVM strategy. This is caused by the reduction of the current ripples. Obviously, all harmonic contents are decreased except the 49^{th} harmonic at this operating point. As a consequence, the total harmonic distortion reduced.

Other comparisons between MCC SVM and the current clamping MCC SVM in terms of THD_0 are listed in Table 5, the relative current trajectories, line current waveforms and harmonic spectrums can be found in appendix. It should be mentioned that the phase inductance is 0.2 p.u. for all operating points. However, the cases exist at operating point 4 and 5 are not be able to treat at the moment, which will be discussed in the following subsection.

See Table 5, the performance of the current clamping MCC SVM is better than the traditional MCC SVM with regard to THD_0 under all treatable operating conditions except operating point 1. This is because that the current clamping is not necessary in this specific condition, zero-crossing case E1 occurs, which has been described in the previous section.

It should be noticed that the most significant improvement of the THD_0 occurs in operating point 6 which has the largest number of zero-crossings. This implies that a better harmonic performance can be given by the functioning of the current clamping strategy.

Table 5 Total harmonic distortion in percent for all treatable operating points

Operating point	MCC SVM THD_0 [%]	Current clamping MCC SVM THD_0 [%]
1	6.9	6.9
2	11.3	8.2
3	6.9	6.7
5	6.5	6.4
6	12.9	7.2
7	7.0	6.3
8	8.0	6.5

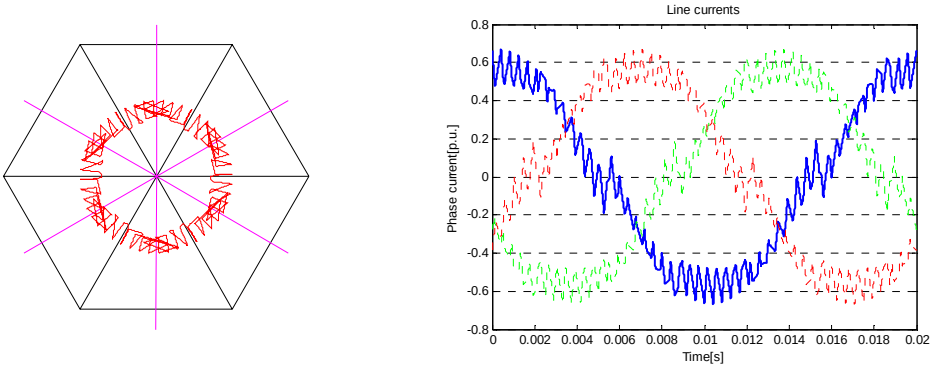

MCC SVM

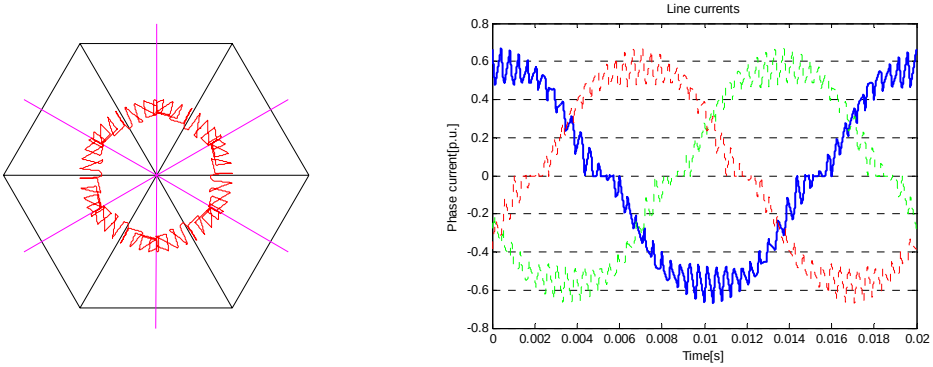

Current clamping MCC SVM

Fig 5.1 Current vector trajectories and line current waveforms at steady-state of the operating point 8, p=48 X_l=0.2 p.u.

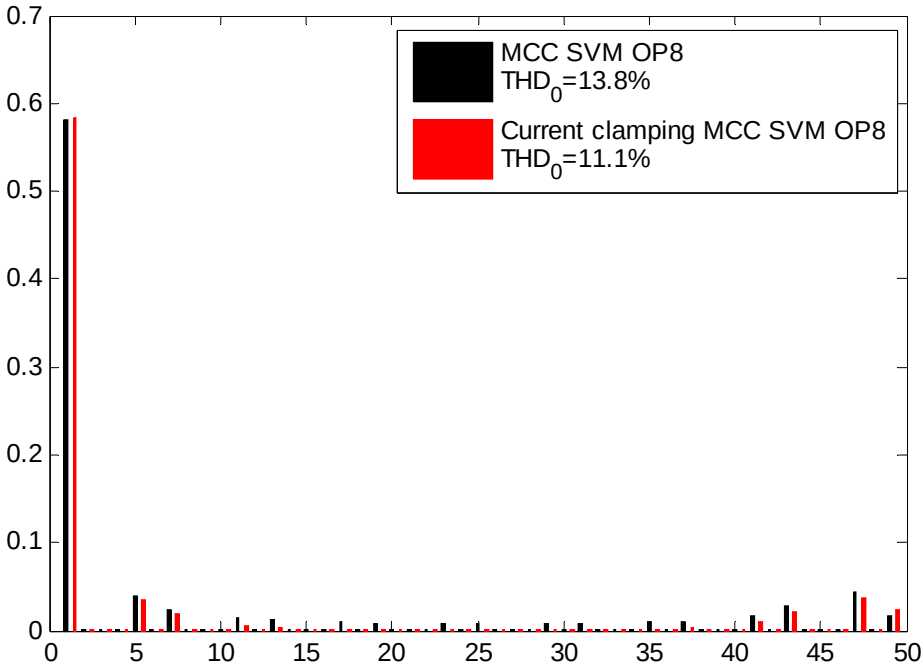

Fig 5.2 Comparison of harmonic performance between MCC SVM and Current clamping MCC SVM at operating point 8, p=48 X_l=0.2 p.u.

5.2 One untreatable case at the moment

There is one special case E5 in operating point 4, shown in Figure 5.3. Unlike case E2, another two commutations are needed after the commutation of the corresponding phase leg in this case where the desired base vector sequence is 1→2→7→4 and an additional commutation of C2 is needed at the end of this modulation interval. This can only be done when IGBTs are used. However, the desired sequence has to be changed as IGBTs are replaced by thyristors in this work.

The commutation of C2 has to be avoided in this case due to that the current vector will finally move to sector 5, which implies that there are two options of the base vector sequence at least: 1-6-5 and 1-0-5, as shown in Figure 5.3, and the clamping of C2 occurs during the selected sequence. It should be mentioned that each treatable case has a unique option with regard to the base vector sequence, and the dead time in such cases is not difficult to calculate. However, in the case E5, the extra degrees of freedom of the base vector sequence makes it a little bit tricky to find a solution.

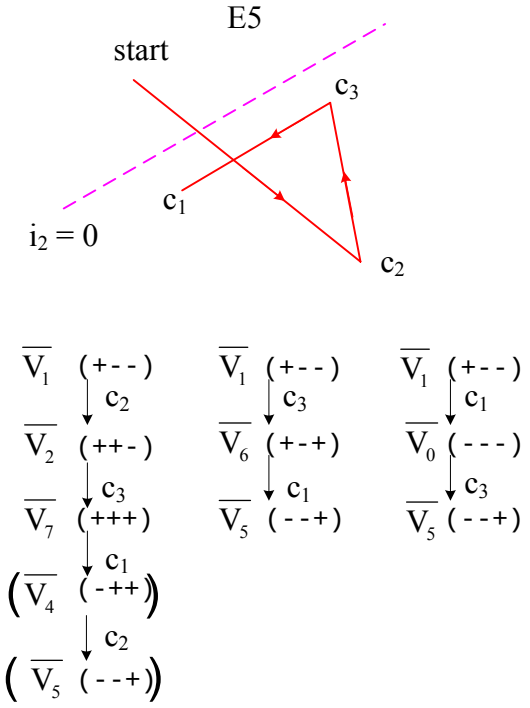

Fig 5.3 One untreatable case at the moment

5.3 Cascaded topology

In all simulations, the actual pulse number is 48 at all operating points, which will give an equivalent pulse number 96. The line current waveforms of the single bridge MCC and the cascaded MCC at operating point 8 are shown in Figure 5.4; a comparison is also made between these two topologies with respect to the harmonic performance and represented in Figure 5.5. See Figure 5.4, as expected, the line current ripple of the cascaded MCC is much lower than the case of a single bridge MCC, which results in a better THD_0. At the same time, in the cascaded MCC, the amplitude of the fundamental output current is almost the same as the single bridge MCC, which is as desired, see Figure 5.5. It should be noticed that the high order harmonics are significantly reduced by the elevated switching frequency. However, the low order harmonics are not improved by the use of the cascaded MCC topology.

The comparisons made between the single-bridge MCC and the cascaded MCC with respect to THD_0 under all treatable operating conditions are shown in Table 6. Apparently, the THD_0 is diminished in accordance with the increasing effective pulse number for all treatable conditions.

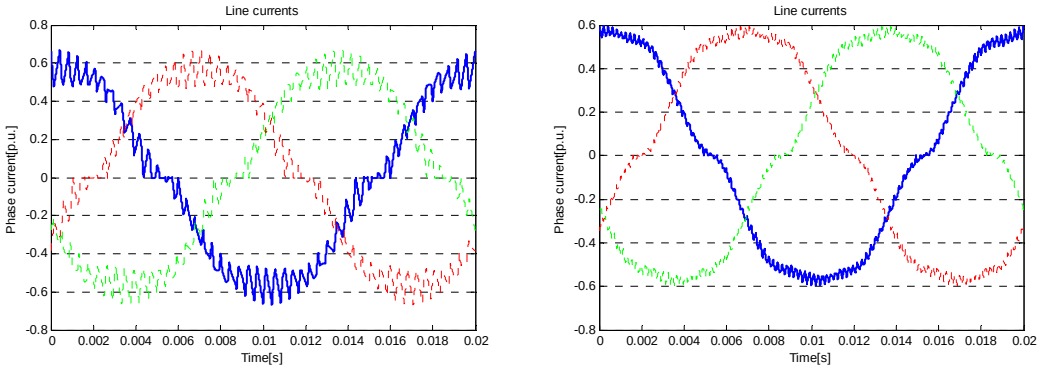

Single bridge MCC Cascaded MCC

Fig 5.4 Line current waveforms of the single bridge MCC and the cascaded MCC at operating point 8, p=48 $X_{l\text{-}single}$ =0.2 p.u., $X_{l\text{-}cascaded}$ =0.4 p.u.

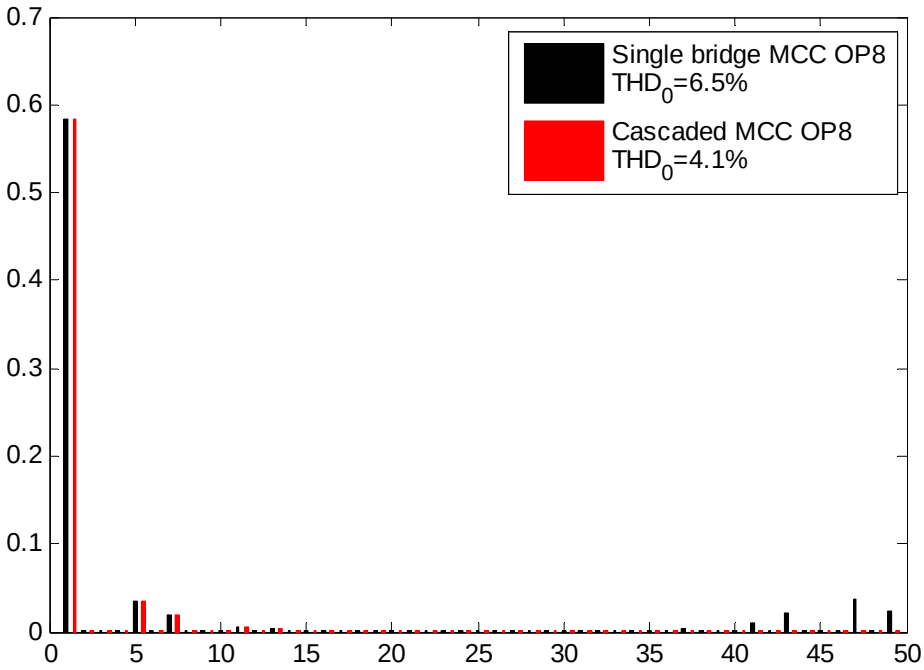

Fig 5.5 Comparison of harmonic performance between single bridge MCC and cascaded MCC at operating point 8, p=48 $X_{l\text{-}single}$ =0.2 p.u., $X_{l\text{-}cascaded}$ =0.4 p.u.

Table 6 Comparisons between single bridge MCC and cascaded MCC with regard to THD_0 (p = 48, $X_{l\text{-}single}$ =0.2 p.u., $X_{l\text{-}cascaded}$ =0.4 p.u.)

Operating point	Single bridge MCC THD_0 [%]	Cascaded MCC THD_0 [%]
1	6.9	1.5
2	8.2	5.8
3	6.7	2.4
5	6.4	3.2
6	7.2	6.6
7	6.3	2.7
8	6.5	4.1

Chapter 6
Conclusion and Future Work

This chapter summarizes the work in this thesis and puts forward future aims in this field.

6.1 Conclusions

A previously proposed current clamping strategy provides a possibility to implement the thyristor-based cycloconverter without having any auxiliary external circuits. As the dead time is predicted according to the current trajectory which calculated by use of the space-vector oriented modulation strategy, the studied converter topology can provide soft switching for all semiconductor valves in all treatable operation points.

By applying this strategy, current reversal can be delayed in the corresponding phase leg and, hence, the soft switching conditions are fulfilled at any instant of the commutation interval. In some cases the desired base voltage vector sequence is not feasible and a new sequence has to be established in order to maximally maintain the desired voltage.

In order to obtain a better harmonic performance, the pulse number is preferably chosen as a multiple of six. It should be mentioned that in all treatable operating points the 5^{th} and 7^{th} harmonics as well as the total harmonic distortion are decreased after using the current clamping strategy. It is becomes especially apparent at operating point 6, where the current ripple is considerable.

Due to the doubled effective pulse number, a better harmonic performance is achieved by the use of the cascaded MCC compared to the single bridge MCC case. High order harmonics are significantly reduced due to this high equivalent switching frequency.

6.2 Future Work

The studied current clamping strategy is based on stopping the current in the corresponding phase leg for a certain dead time, this result in the difficulties to decide the new base vector sequence and the concerned duty ratio in some discussed special cases which are not able to treat at the moment. A universal algorithm is required to solve all cases. Furthermore, the implementation of the predictor for such a strategy is not easy as the requirement of all parameters of a time-variant system. Therefore, a possible better solution is to arrange the base vector sequence in a favorable way that all zero-crossing cases are as in the case E4.

Appendix
All Simulation Results

In this appendix, simulation results for all treatable operating points will be shown. The phase inductance of all single-bridge MCC simulations is 0.2 p.u.. In the cases of cascaded MCC, the phase inductance is increased to 0.4 p.u.. All THD_0s are referred to the output line current. Pulse number for all simulations is 48.

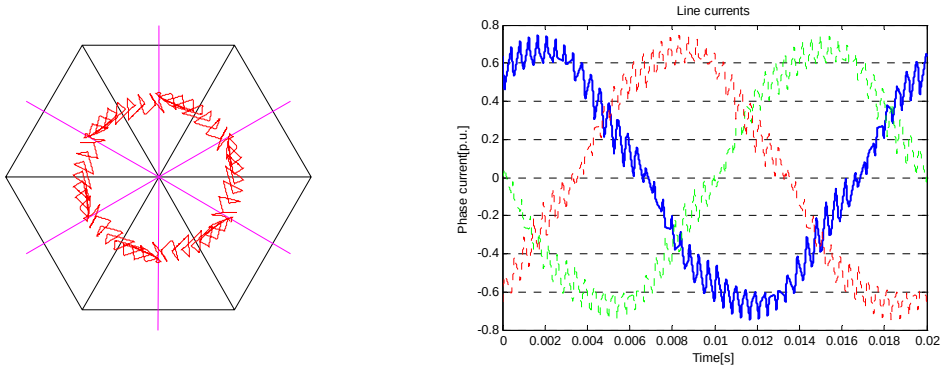

MCC SVM

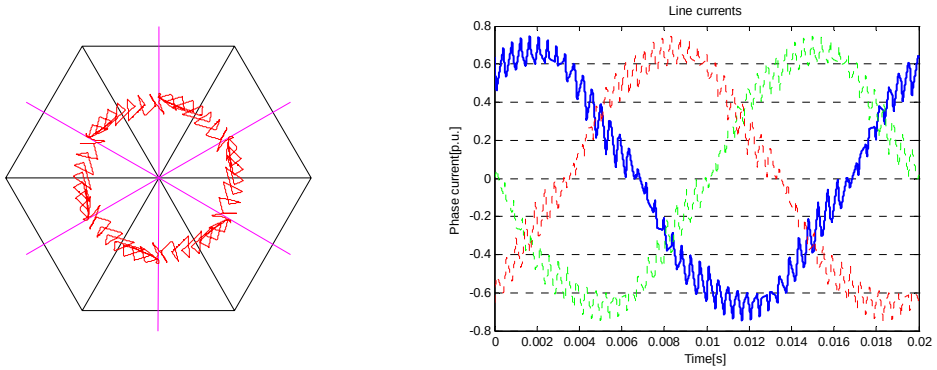

Current clamping MCC SVM

Fig A1 Current vector trajectories and line current waveforms at steady-state at operating point 1.

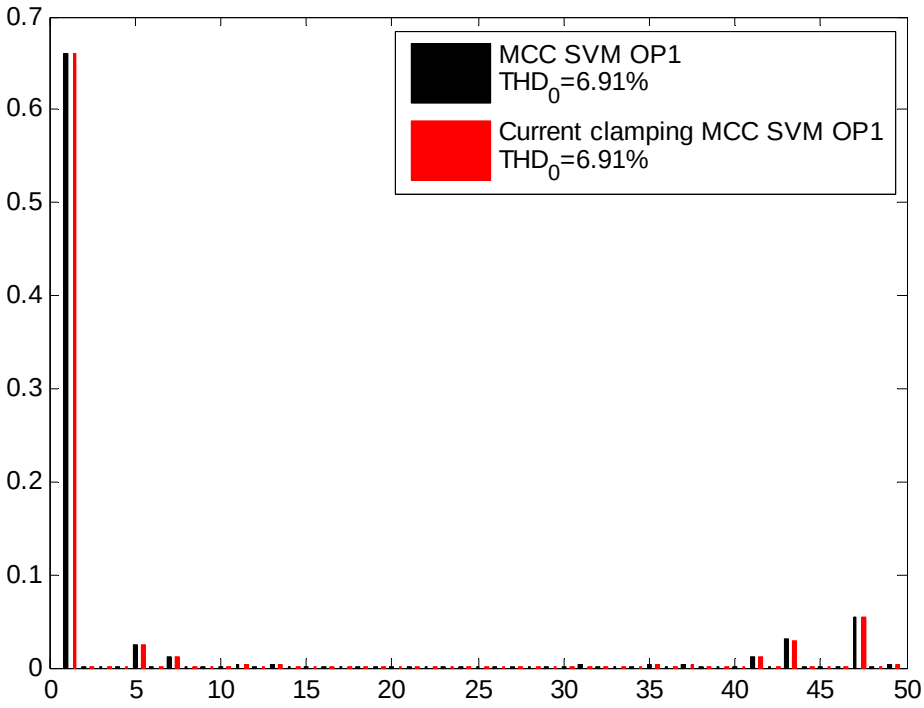

Fig A2 Comparison of harmonic performance between MCC SVM and Current clamping MCC SVM at operating point 1.

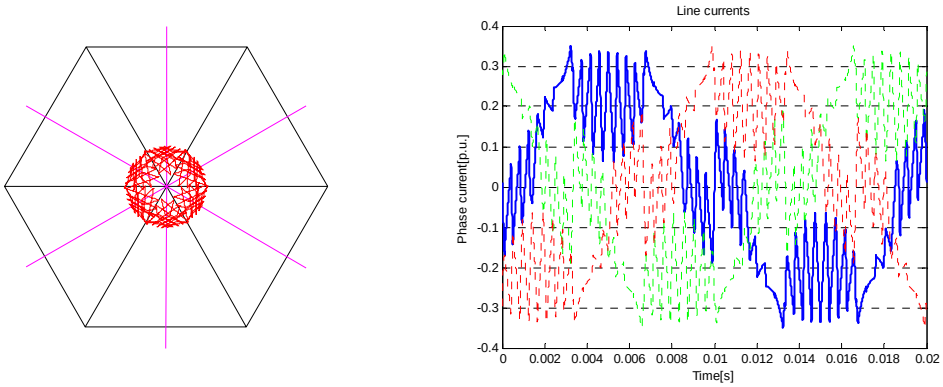

MCC SVM

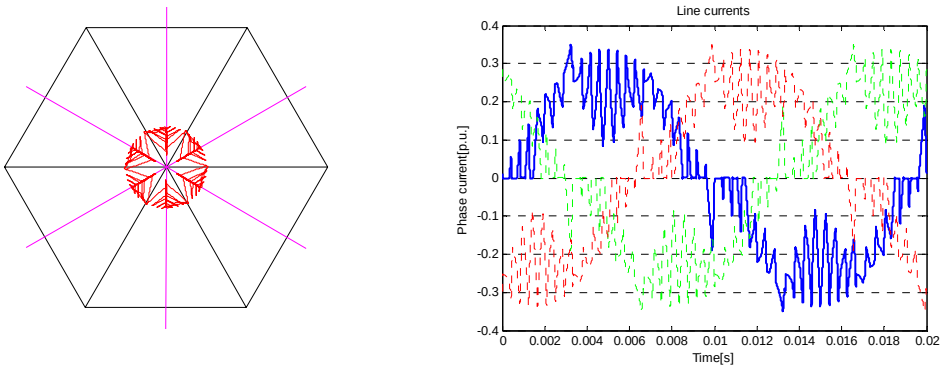

Current clamping MCC SVM

Fig A3 Current vector trajectories and line current waveforms at steady-state at operating point 2.

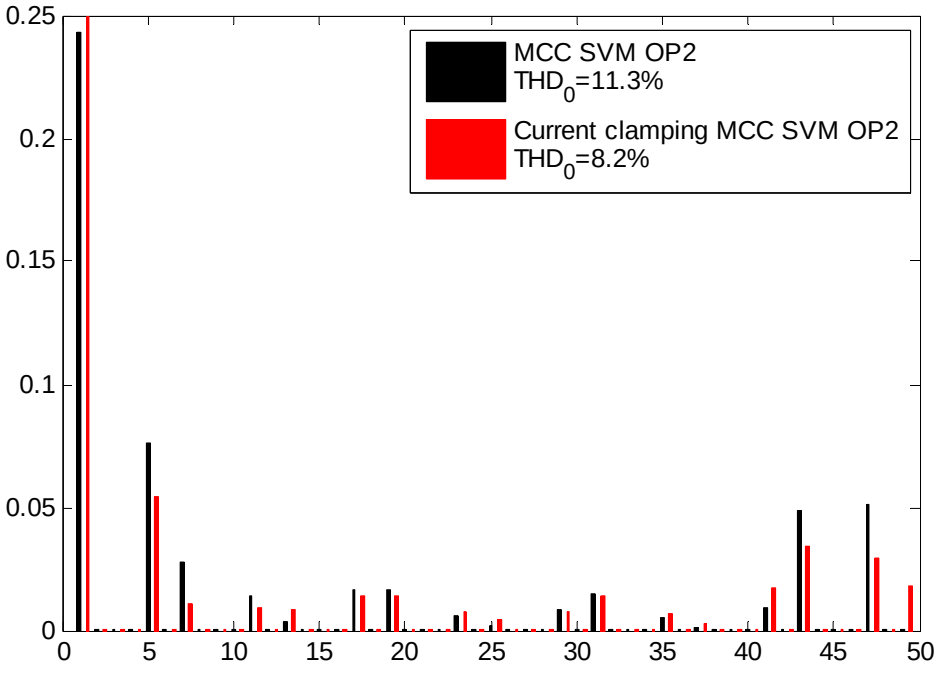

Fig A4 Comparison of harmonic performance between MCC SVM and Current clamping MCC SVM at operating point 2.

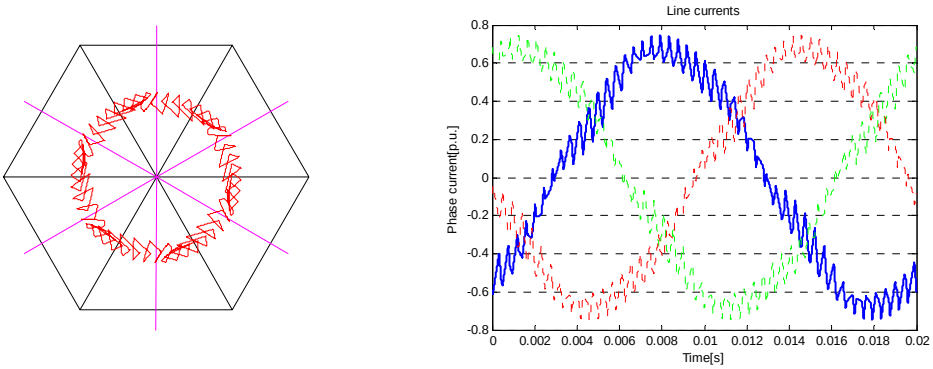

MCC SVM

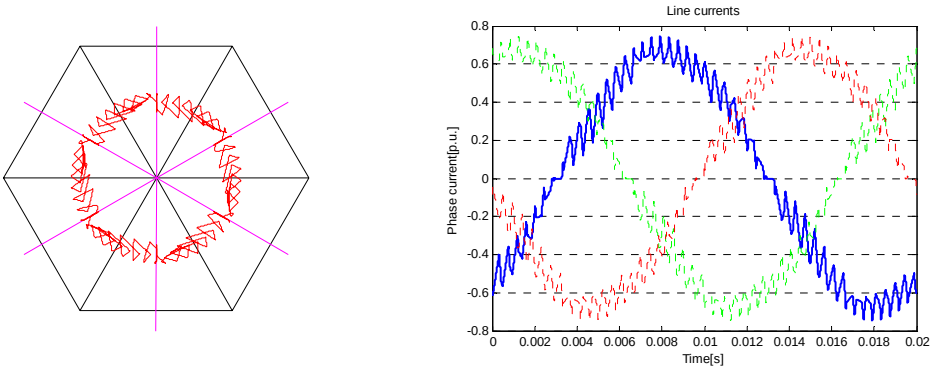

Current clamping MCC SVM

Fig A5 Current vector trajectories and line current waveforms at steady-state at operating point 3.

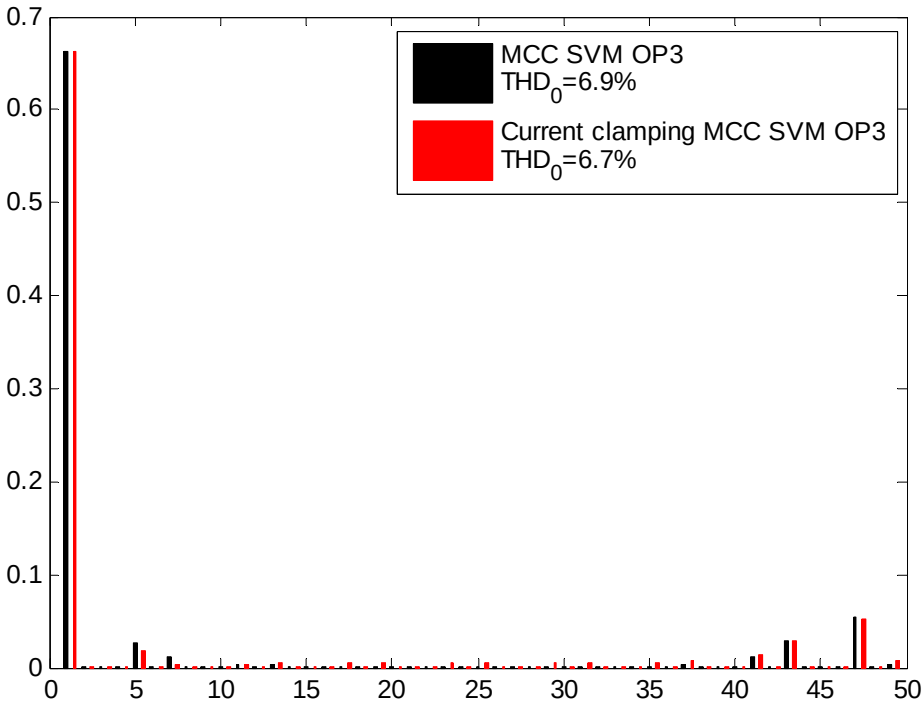

Fig A6 Comparison of harmonic performance between MCC SVM and Current clamping MCC SVM at operating point 3.

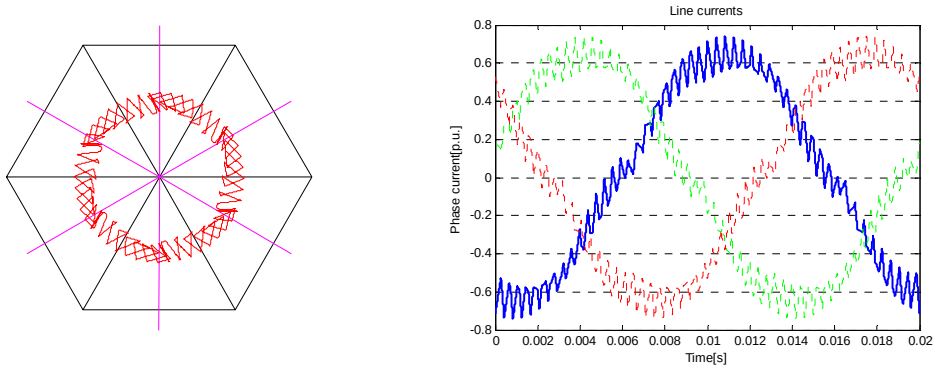

MCC SVM

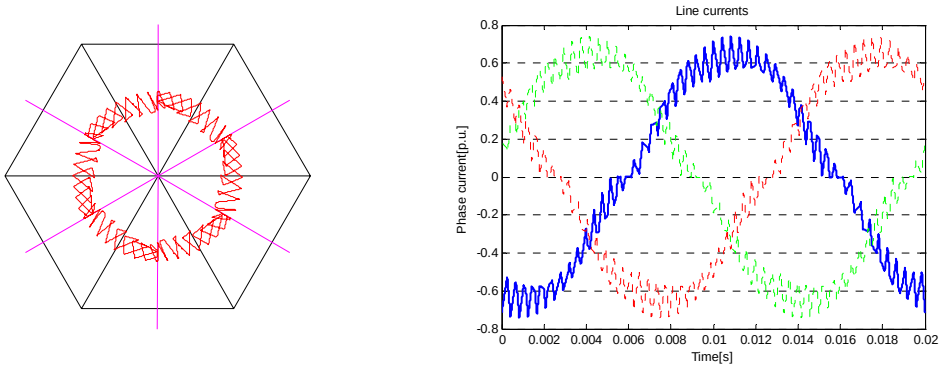

Current clamping MCC SVM

Fig A7 Current vector trajectories and line current waveforms at steady-state at operating point 5.

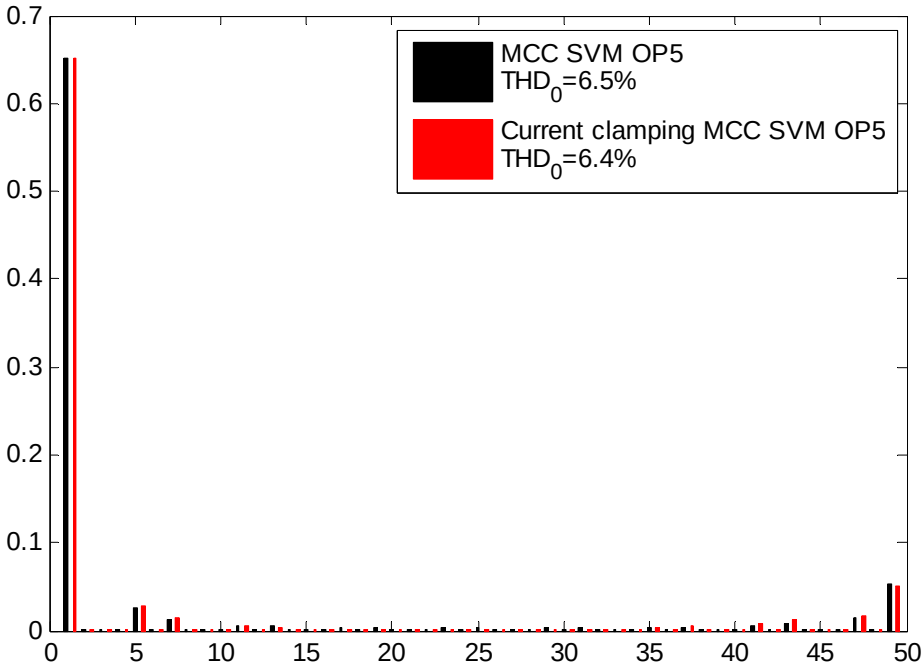

Fig A8 Comparison of harmonic performance between MCC SVM and Current clamping MCC SVM at operating point 5.

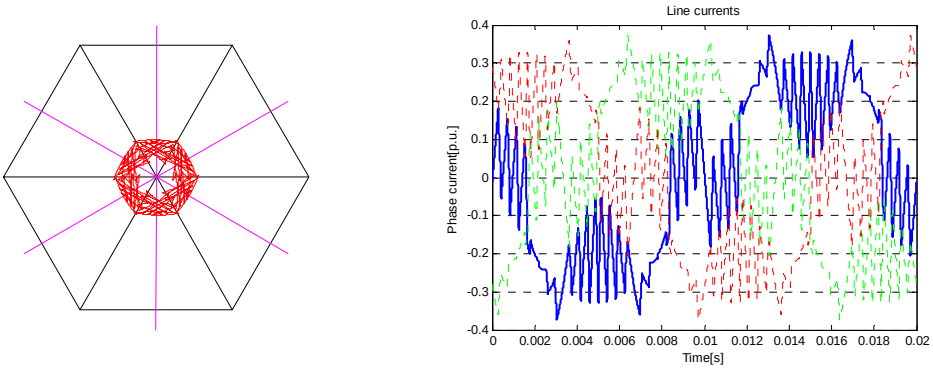

MCC SVM

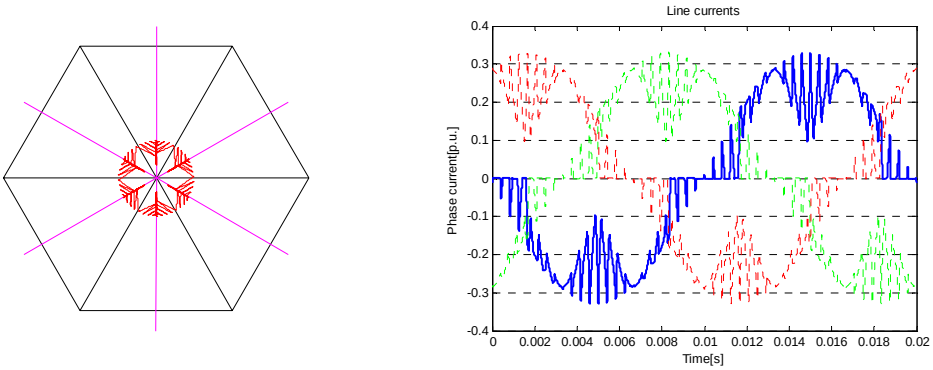

Current clamping MCC SVM

Fig A9 Current vector trajectories and line current waveforms at steady-state at operating point 6.

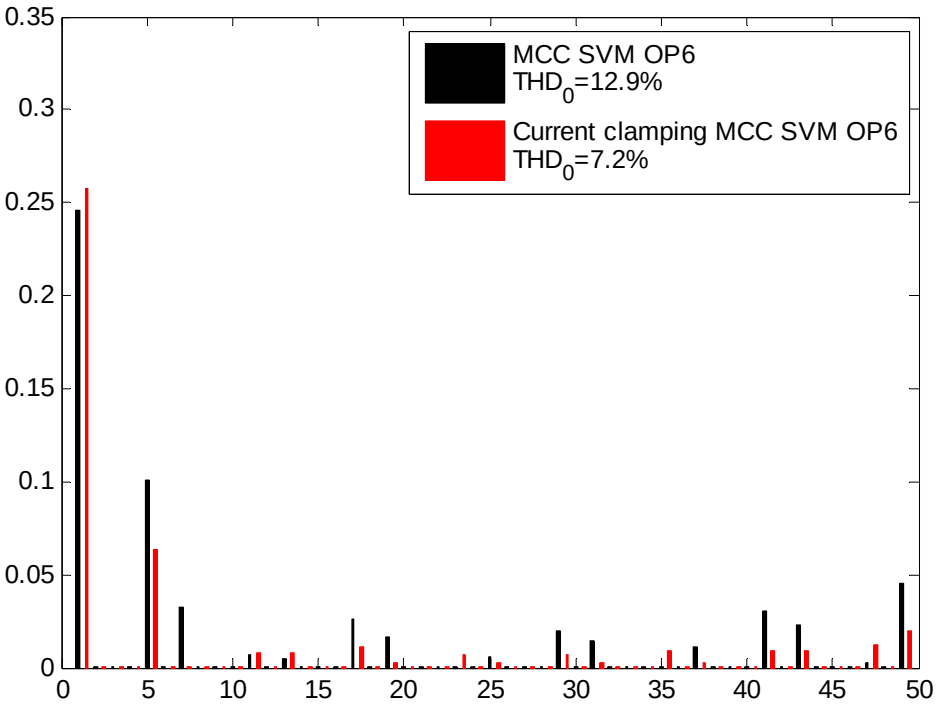

Fig A10 Comparison of harmonic performance between MCC SVM and Current clamping MCC SVM at operating point 6.

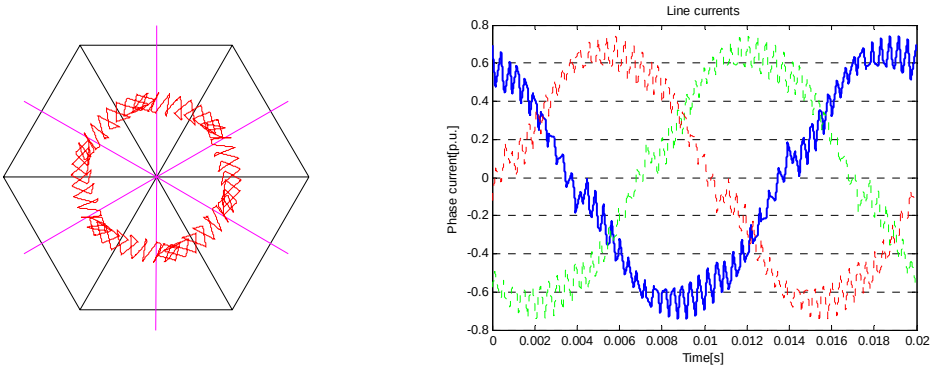

MCC SVM

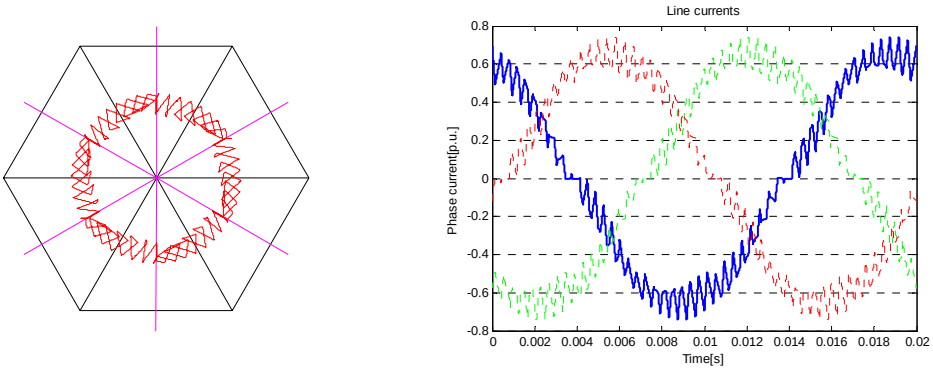

Current clamping MCC SVM

Fig A11 Current vector trajectories and line current waveforms at steady-state at operating point 7.

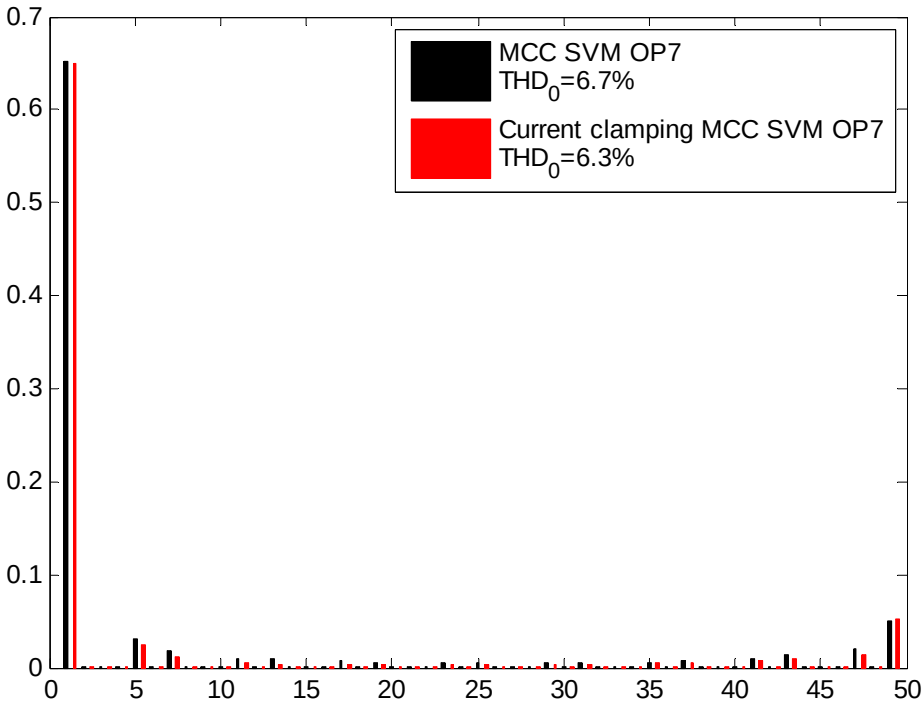

Fig A12 Comparison of harmonic performance between MCC SVM and Current clamping MCC SVM at operating point 7.

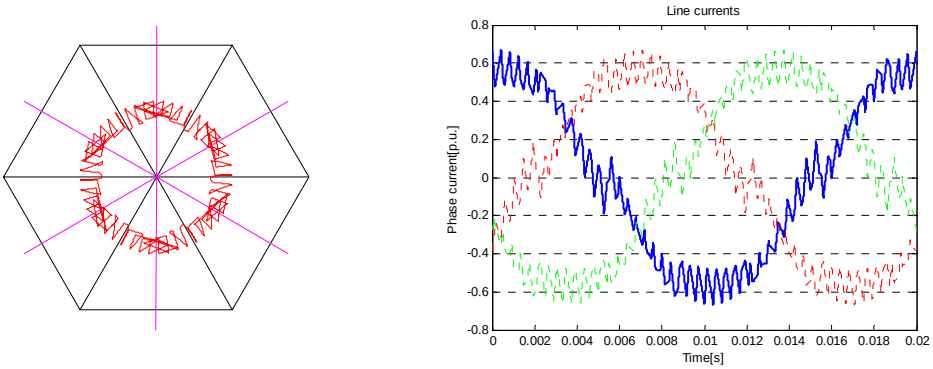

MCC SVM

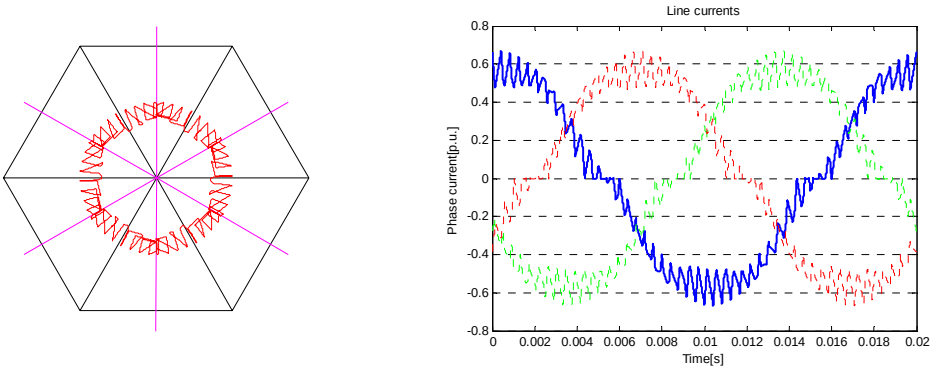

Current clamping MCC SVM

Fig A13 Current vector trajectories and line current waveforms at steady-state at operating point 8.

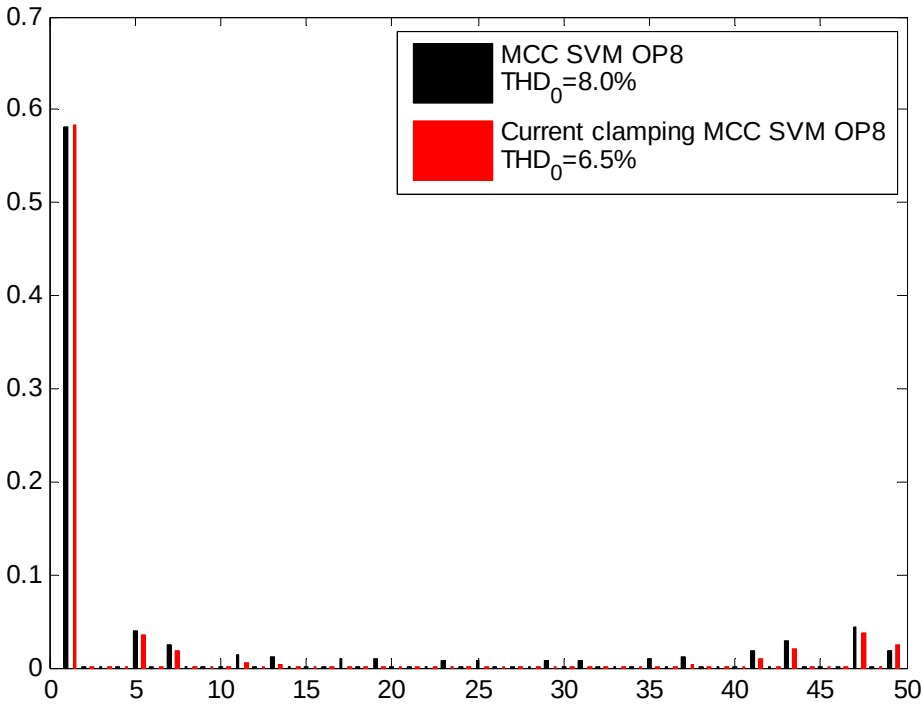

Fig A14 Comparison of harmonic performance between MCC SVM and Current clamping MCC SVM at operating point 8.

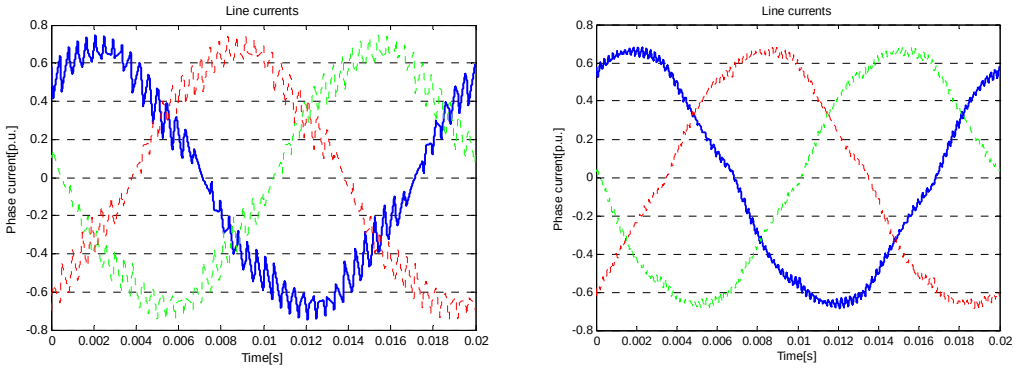

Single bridge MCC Cascaded MCC

Fig A15 Line current waveforms of the single bridge MCC and the cascaded MCC at operating point 1.

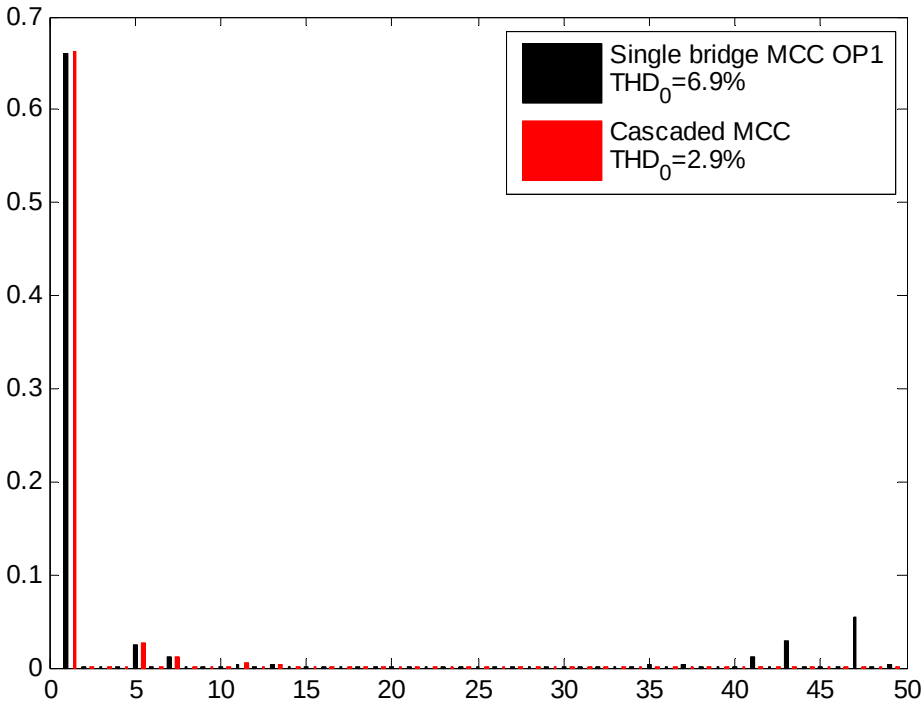

Fig A16 Comparison of harmonic performance between single bridge MCC and cascaded MCC at operating point 1.

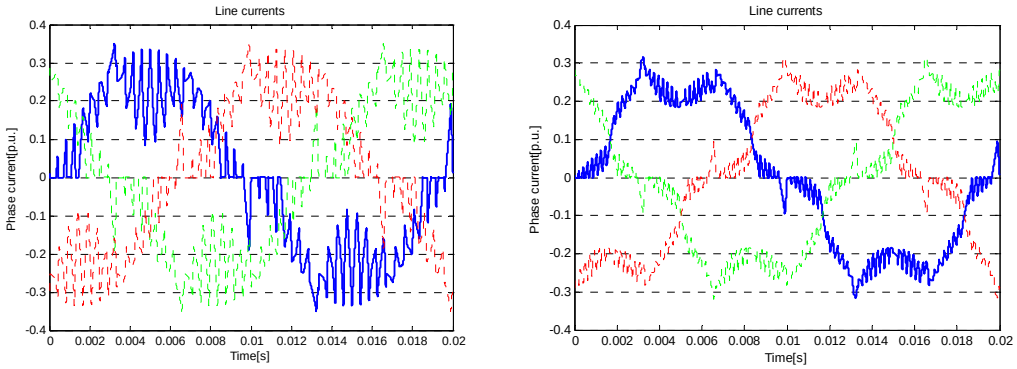

Single bridge MCC Cascaded MCC

Fig A17 Line current waveforms of the single bridge MCC and the cascaded MCC at operating point 2.

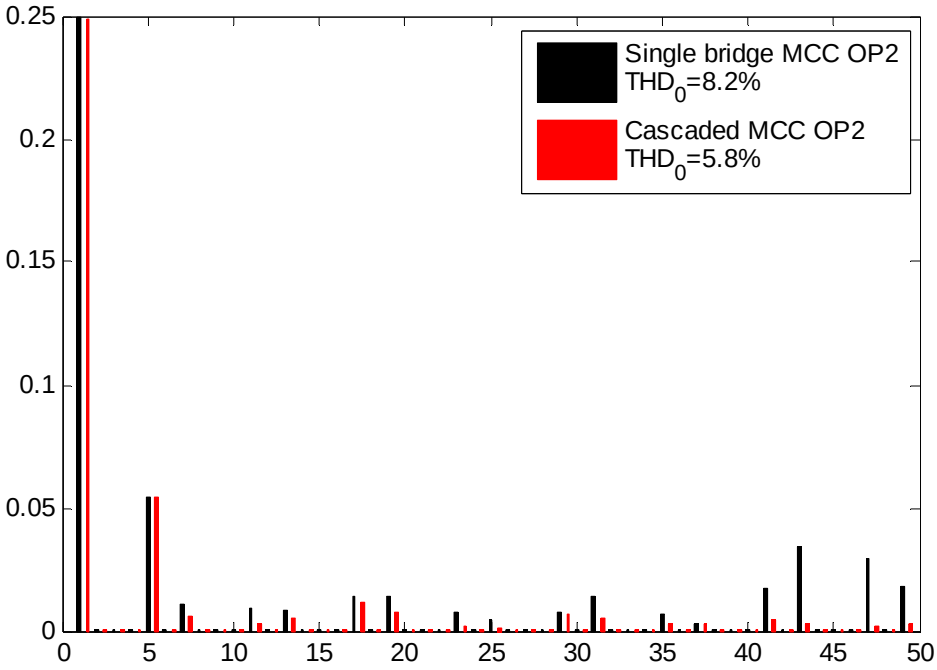

Fig A18 Comparison of harmonic performance between single bridge MCC and cascaded MCC at operating point 2.

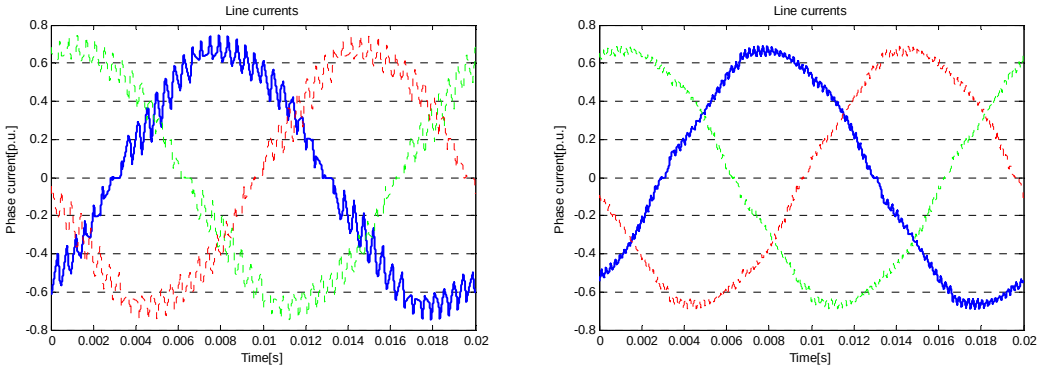

Single bridge MCC Cascaded MCC

Fig A19 Line current waveforms of the single bridge MCC and the cascaded MCC at operating point 3.

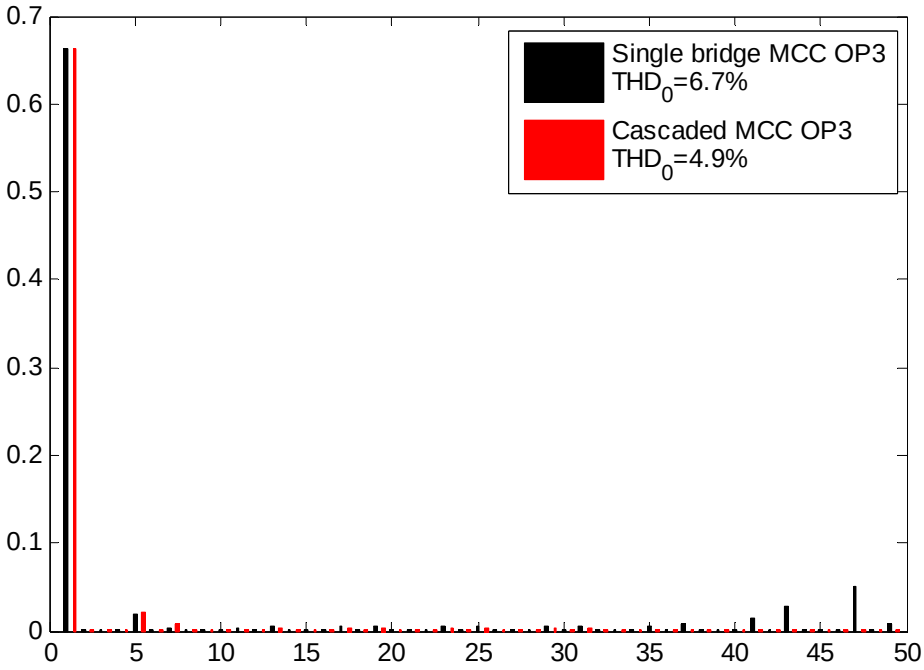

Fig A20 Comparison of harmonic performance between single bridge MCC and cascaded MCC at operating point 3.

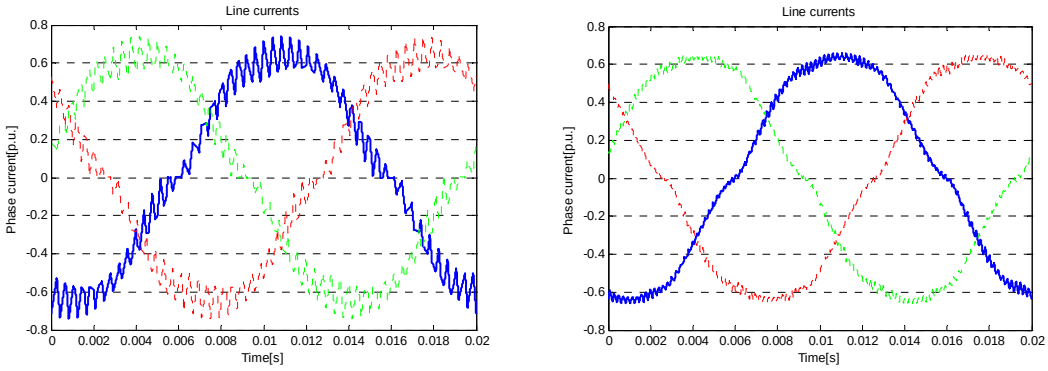

Single bridge MCC Cascaded MCC

Fig A21 Line current waveforms of the single bridge MCC and the cascaded MCC at operating point 5.

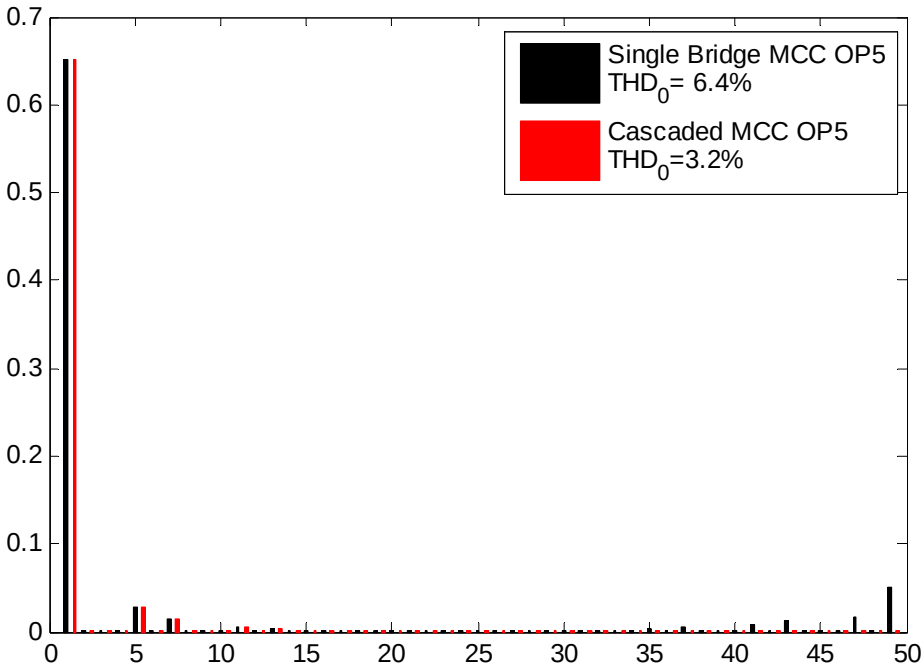

Fig A22 Comparison of harmonic performance between single bridge MCC and cascaded MCC at operating point 5.

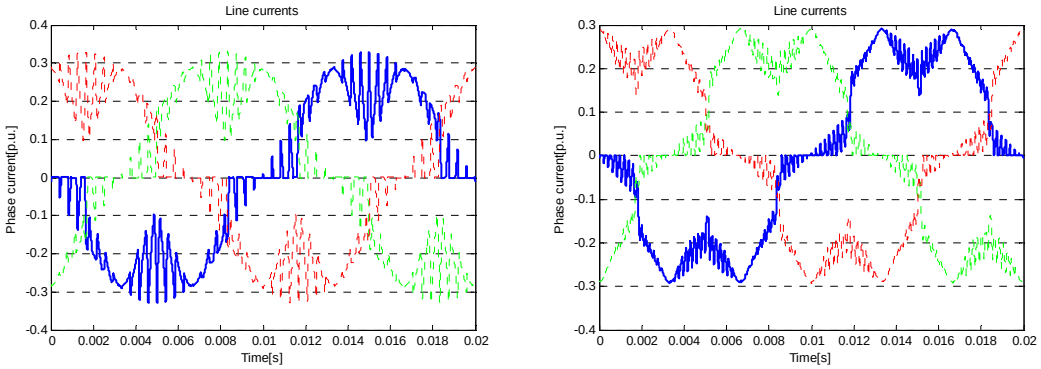

Single bridge MCC Cascaded MCC

Fig A23 Line current waveforms of the single bridge MCC and the cascaded MCC at operating point 6.

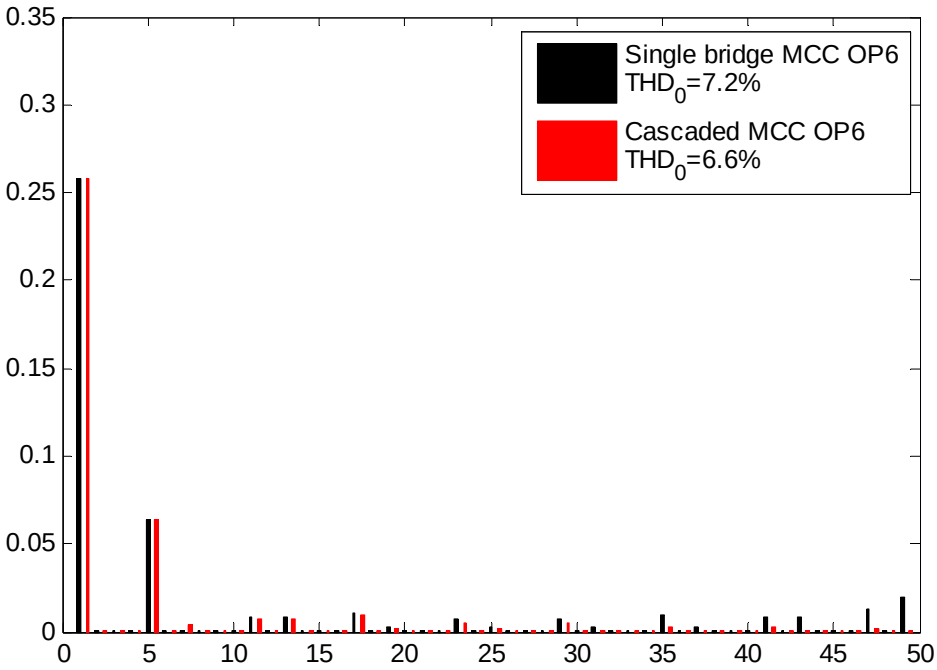

Fig A24 Comparison of harmonic performance between single bridge MCC and cascaded MCC at operating point 6.

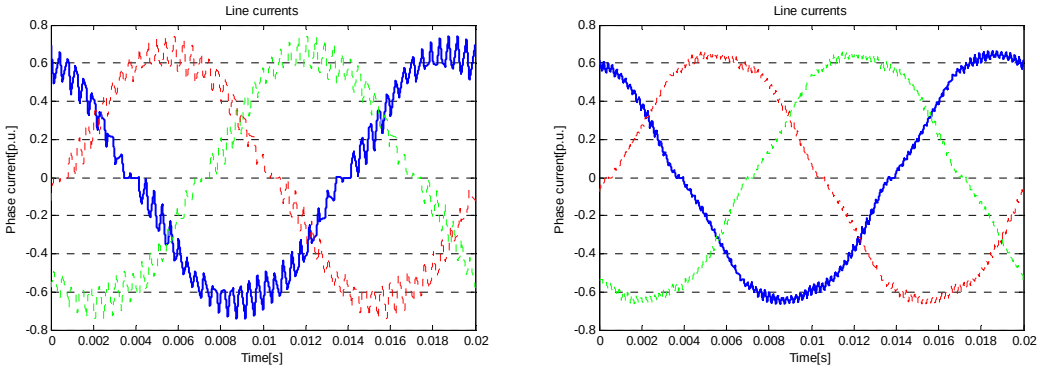

Single bridge MCC Cascaded MCC

Fig A25 Line current waveforms of the single bridge MCC and the cascaded MCC at operating point 7.

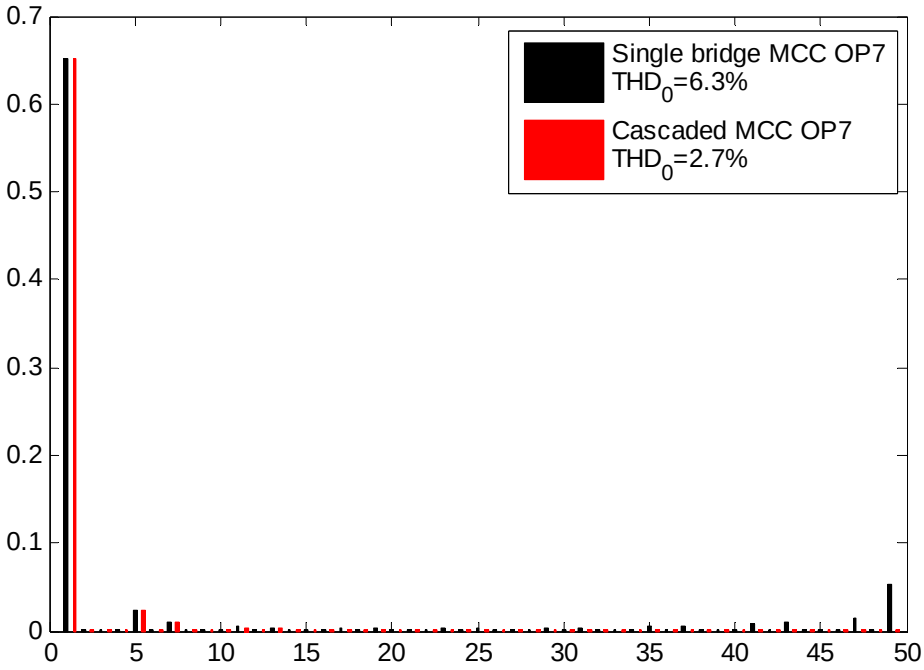

Fig A26 Comparison of harmonic performance between single bridge MCC and cascaded MCC at operating point 7.

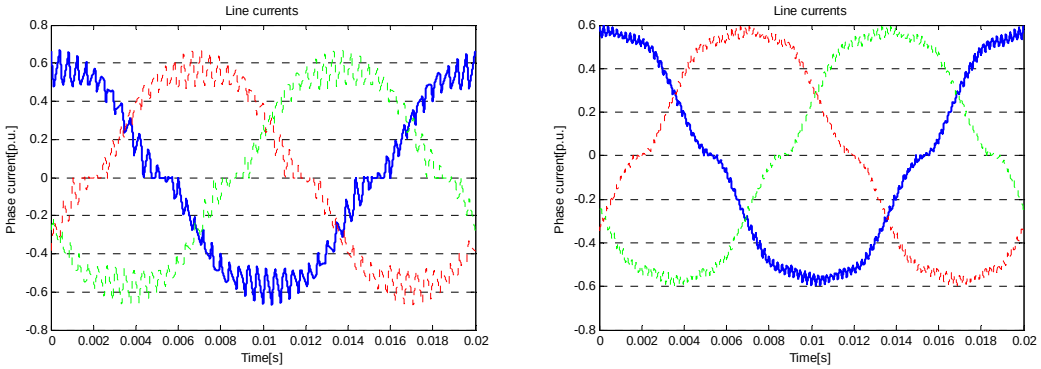

Single bridge MCC Cascaded MCC

Fig A27 Line current waveforms of the single bridge MCC and the cascaded MCC at operating point 8.

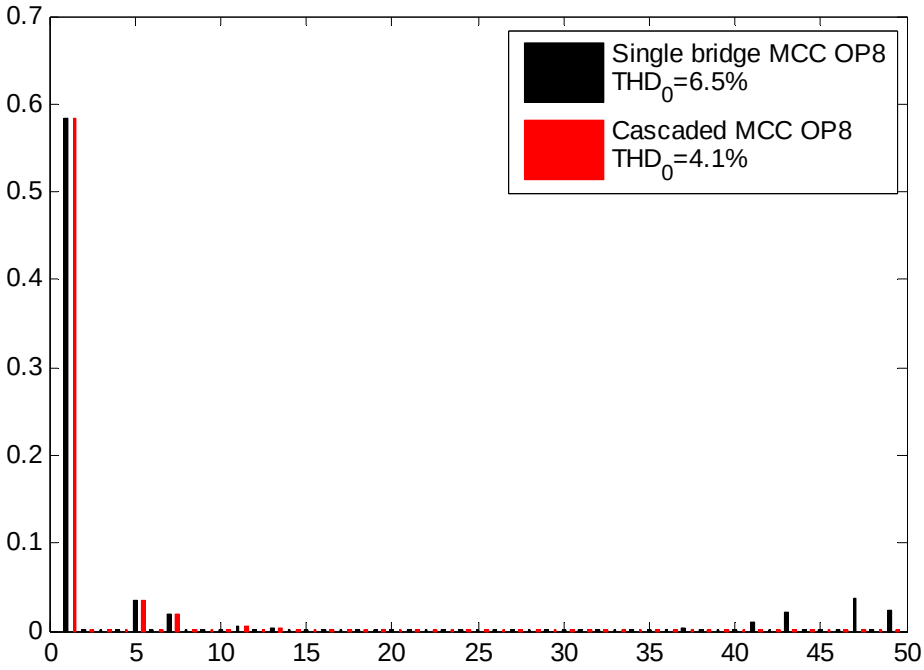

Fig A28 Comparison of harmonic performance between single bridge MCC and cascaded MCC at operating point 8.

Reference

[1] Staffan Norrga, “On Soft-Switching Isolated AC/DC Converters without Auxiliary Circuit.” Doctoral Thesis in Royal Institute of Technology, 2005

[2] Staffan Norrga, “Modulation Strategies for Mutually Commutated Isolated Three-Phase Converter Systems.” PESC 2005, pp.2736-2743

[3] D. Geahame Holmes, Thomas A. Lipo, “Pulse Width Modulation for Power Converters - Principles and Practice”, IEEE Series on Power Engineering, 2003

[4] Stephan Meier, Staffan Norrga, Hans-Peter Nee, “Modulation Strategies for a Mutually Commutated Converter System in Wind Farms.” Proceedings EPE 2007